Aerostructural Wing Optimization Using a Surrogate Model of the Structure in a Coupled Adjoint Formulation

Joshua E. Fontana* and Pat Piperni†
Clarkson University, Potsdam, NY 13699

Zhi Yang‡ and Dimitri J. Mavriplis§
University of Wyoming, Laramie, WY 82071

As the number of disciplines included in the multidisciplinary design optimization (MDO) process continues to increase, it is envisioned that some of the disciplinary tools will take the form of surrogate models, while others remain physics-based, depending on the requirements and stage of the design process. To simulate this in the context of an aerostructural optimization of an aircraft wing, the work presented herein features a high-fidelity aerodynamic flow solver, while a surrogate is employed to model the wing structure. This approach includes the evaluation of the sensitivities of both the aerodynamic and structural disciplines, using a coupled-adjoint formulation to enable gradient-based optimization. An important aspect of the method is that the surrogate is trained only once, prior to the optimization, and held fixed throughout. The surrogate in effect parameterizes the structural design process, and outputs the weight and stiffness of an optimized structure, given inputs of geometry parameters and sizing loads. To minimize the number of surrogate inputs and enable the representation of the entire structural design space, parameterized loads are used to build the surrogate. The method is applied to the optimization of the NASA Common Research Model (CRM), illustrating the effectiveness of the new approach.

Nomenclature

A	=	vector of beam cross sectional areas
$A_{beam}^{(i)}$	=	beam cross sectional area for beam segment i
$\bar{A}_n$	=	vector of Fourier coefficients for a parameterized lift distribution
A_n	=	concatenation of $\bar{A}_n$ and $(x/c)_{cp}$ vectors, and wing C_L

Revised from paper 2023-3796 at AIAA AVIATION 2023 Forum, San Diego, CA and Online, June 12 - 16.

*PhD Candidate, AIAA Student Member; email: fontanj@clarkson.edu
†Associate Professor, AIAA Member; email: ppiperni@clarkson.edu
‡Research Scientist, AIAA Member; email: zyang@scientific-sims.com
§Professor, AIAA Associate Fellow; email: mavriplis@uwyo.edu

AR	=	wing aspect ratio
B	=	vector of beam parameters for sized wing structure
b	=	wing span
c	=	local chord (unless otherwise noted)
$C_{m,QC}$	=	sectional pitching moment coefficient, about quarter-chord
C_m	=	sectional pitching moment coefficient
c_{av}	=	average chord of the wing
C_l	=	sectional lift coefficient
C_L	=	aircraft lift coefficient
C_D	=	aircraft drag coefficient
c_t	=	thrust specific fuel consumption
C_p	=	pressure coefficient
D	=	vector of all design variables (unless otherwise noted)
D_G	=	NSU3D geometric input parameters derived from design variables
D_0	=	design variables that are shared between aerodynamic and structural disciplines, a subset of D
D_α	=	design variable for angle-of-attack
F_B	=	discrete forces derived from CFD sectional forces to be applied to beam model
F_{st}	=	sectional force coefficients and chords at a set of spanwise stations
F_T	=	total force coefficients
G	=	mesh deformation residuals
I_y	=	vector of beam second moments of area about the out-of-plane bending axis
$Iy_{beam}^{(i)}$	=	beam second moment of area about the out-of-plane bending axis for beam segment i
I_z	=	vector of beam second moments of area about the in-plane bending axis
$Iz_{beam}^{(i)}$	=	beam second moment of area about the in-plane bending axis for beam segment i
J	=	vector of beam polar second moments of area
$J_{beam}^{(i)}$	=	beam polar second moment of area for beam segment i
K	=	stiffness matrix of the beam model
L/D	=	lift-to-drag ratio
t	=	thicknesses of structural shell elements in S4Wing model
OBJ	=	objective function (unless otherwise noted)
R	=	flow residuals (unless otherwise noted)
Re	=	Reynolds number

R^2	=	coefficient of determination
S	=	structural residuals
t/c	=	thickness to chord ratio at several spanwise stations
u	=	vector of structural state variables
u_{TB}	=	beam sectional twist and bending deflections
$\hat{u}_{TB}$	=	sectional wing deflections used for CFD analysis
u_s	=	nodal deflections for S4Wing structural model
V_∞	=	true airspeed
$W_{A/C}$	=	aircraft maximum take-off weight
W_f	=	fuel weight
W_{other}	=	the total weight of every part of the aircraft other than the structural wing weight
W_{WS}	=	wing structural weight for one wing, excluding the center wingbox
$W_{WS,center}$	=	center wingbox structural weight for one wing
x	=	mesh coordinates
x_B	=	vector of coordinates of beam elastic axis for sized wing structure
$xB_x^{(i)}$	=	x coordinate of beam elastic axis point (i)
$xB_y^{(i)}$	=	y coordinate of beam elastic axis point (i)
$xB_z^{(i)}$	=	z coordinate of beam elastic axis point (i)
$(x/c)_{cp}$	=	center-of-pressure chordwise location at a given spanwise wing station
x_{sf}	=	wing surface coordinates from updated design variables and structural deflections
β_1	=	weighting factor on the first term of the objective
β_2	=	weighting factor on the second term of the objective
$\Delta\Lambda_{TE}$	=	change in wing trailing-edge sweep at the kink station
η	=	non-dimensional spanwise coordinate based on centerline (0.0 at centerline, 1.0 at tip)
η'	=	non-dimensional spanwise coordinate based on wing root (0.0 at root, 1.0 at tip)
$\Lambda_{TE,ibk}$	=	wing trailing-edge sweep inboard of trailing-edge kink station
λ_X	=	adjoint vector associated with variable X
θ	=	non-dimensional spanwise coordinate for the Glauert Fourier series
σ	=	stresses in S4Wing structural model
$(\cdot)^c$	=	denotes the cruise case
$(\cdot)^s$	=	denotes the sizing load case
ω	=	vector of aerodynamic state variables

I. Introduction

A. Background

The aerostructural optimization of aircraft wings typically involves a large number of design variables and constraints, as well as requiring advanced tools and expertise from multiple engineering disciplines. To address these challenges, the numerous approaches that have been developed over the years have focused on three general areas of development [1]: i) sensitivity analysis to enable efficient gradient-based optimization, ii) approximation modeling to mitigate long run times, and iii) problem decomposition to accommodate organizational constraints. From the point of view of computational efficiency, it has been shown that gradient-based optimization algorithms, used in conjunction with the coupled-adjoint technique for computing gradients, provide the greatest degree of scalability to large problems [2, 3]. However, implementing such approaches in an industrial setting can be challenging from an organizational perspective, especially as the number of disciplines considered is increased. In particular, the validation of system-level results based on the inputs of a diverse community of experts can be a significant difficulty in large-scale MDO initiatives [4]. Specialized tools are typically developed by different engineering departments, and the inherent complexity of aircraft design demands a high degree of knowledge and tool specialization. In such an environment, the identification of design responsibilities and the sharing of disciplinary tools must be done in a careful manner, to ensure their proper application at all stages of design [5].

These organizational challenges can be mitigated by the use of a distributed MDO architecture, in which the overall optimization problem is decomposed into disciplinary sub-optimizations [6]. However, distributed methods are often less efficient than monolithic architectures [7, 8]. Some researchers have endeavored to mitigate this issue by only using sub-optimizations for less costly disciplines, while leaving expensive disciplines to be optimized by the system level optimizer [9]. However, the use of any sub-optimization in an MDO architecture increases the complexity of gradient-based methods at the system level, because coupled post-optimality sensitivities (CPOS) are required [10]. This increased complexity, together with the aforementioned efficiency penalty, make distributed architectures less attractive, yet they continue to be the choice of industry due to the great need to build upon existing disciplinary procedures and organizational structures [11].

The use of surrogate models is another common way to enable disciplinary separation and autonomy. Surrogate models are often used as an effective way to share disciplinary tools , as the models can be validated a priori by disciplinary experts and provided to end users for a target application. However, many of the surrogate-based MDO methods that have been studied in the literature are adaptive in nature [12–15], in which the surrogate must be updated with high-fidelity data during the course of the multidisciplinary optimization procedure. This demands that the high-fidelity disciplinary tools be integrated into the MDO framework, thereby largely nullifying the disciplinary autonomy afforded by the use of surrogates.

One the other hand, so-called one-shot surrogate modeling methods have also been explored, in which the surrogate model is trained on an initial set of sample data and held constant during the optimization (e.g. [16]). While these methods are not as efficient as adaptive methods, they facilitate collaboration in an industrial environment, as the end-user is freed from the task of running the high-fidelity process that the surrogate approximates. There is also a middle ground in sequentially sampled space-filling methods, in which sample points are added sequentially to fill the input space [15]. Such techniques would also facilitate interdepartmental collaboration, so long as all of the sampling is performed prior to the MDO process.

The benefits to interdisciplinary collaboration are also precluded, however, in methods which use a surrogate to approximate the entire coupled system (e.g. [12, 14, 17–19]). In that case, the training process to collect data for the surrogate must integrate the high-fidelity tools of all disciplines, which again diminishes disciplinary autonomy.

Therefore, for a surrogate-based MDO strategy to truly cater to the organizational challenges of an industrial setting, the surrogates must be used in a way that aligns with disciplinary and organizational boundaries. Since engineering departments already have well-established methods for performing single-discipline optimizations in their area of expertise, using a surrogate to approximate a disciplinary sub-optimization in the MDO process is a natural choice. Indeed, many researchers have done this for various disciplines [13, 20–23]. This technique has the additional benefit of removing that discipline's local variables and constraints from the system-level optimization problem, which has been shown to be beneficial to the system convergence in the context of the Asymmetric Subspace Optimization architecture [10]. These benefits are ordinarily the appeal of distributed MDO architectures, but, with the use of a surrogate model generated a priori, the architecture of an aerostructural optimization process can remain monolithic, if the disciplinary sub-optimization of one of the two disciplines is replaced by a surrogate model. There is added cost to train the surrogate prior to the MDO process, however.

Several studies in the literature utilize one-shot surrogate models of a structural sizing process to approximate the structural weight [20, 21], but very few have approximated the stiffness of the sized wing structure with such a model. The work of Chaussée and Dervault is a notable exception [24], but they have not employed their stiffness model in an aerostructural optimization process. The stiffness is essential if a fully coupled multidisciplinary analysis is to be used in the sizing of the wing structure, or in subsequent cruise case evaluations.

Aside from collaboration considerations, computational efficiency is also an essential factor, which can often be afforded by the use of gradients computed by the adjoint method. However, many gradient-based methods do not make use of surrogate models [25–28], and many surrogate-based methods do not make use of gradients [18, 29, 30]. Some researchers have sought to take advantage of both by using gradient information to enrich surrogate models [23, 31–34]. Others have used surrogate-based methods to provide a starting point for a gradient-based optimization [32]. However, to the best of our knowledge, none have used a surrogate model embedded in a coupled-adjoint formulation for gradient-based optimization.

In light of the aforementioned advantages of gradient-based optimization and surrogate modeling for interdisciplinary collaboration, the methodology proposed herein utilizes a one-shot surrogate model to replace a structural sub-optimization process, which is embedded in a coupled-adjoint formulation to compute sensitivities. The surrogate produces both the weight and stiffness of the sized wing structure to allow fully coupled interactions. In this way, the proposed method aims to perform fully coupled aerostructural optimization, and preserve disciplinary autonomy and validation while enabling an efficient gradient-based optimization method for large-scale design problems. There also exists synergy in this combination that mitigates some disadvantages of each technique alone. For example, the structural discipline local variables and constraints are eliminated from the aerostructural optimization problem, as in a distributed architecture, yet there is no need to compute coupled post-optimality sensitivities (CPOS) as part of the adjoint formulation, since the surrogate completely replaces the structural sub-optimization.

Additional details and motivations of the new method, and its target application within the industrial design cycle, were presented [35], and are summarized in section II.B.1. The current paper presents more specifics of the coupled-adjoint formulation for this method, describes the construction of a complete one-shot surrogate model for computing both weight and stiffness of a sized wing structure, and applies the proposed method to the aerostructural optimization of a flexible wing.

II. Methodology

A. Target Design Stage

In the development of any new tool for aircraft design, it is important to identify the stage of the design process the new tool aims to benefit. It is well known that the most critical phases of design are the conceptual and preliminary design stages, as these have the largest impact on both the performance and economic viability of new aircraft. To this end, the work presented here targets the preliminary design stage, in which it is imperative to have a time-efficient multidisciplinary optimization (MDO) capability that can support evolving design requirements, whilst also facilitating interdepartmental collaboration. In this work, high-fidelity computational fluid dynamics (CFD) is retained for the aerodynamic simulation, whereas a surrogate is used to represent the structural discipline. Such a setup may be used in an aerodynamics department to optimize the wing aerodynamics, while taking into account the impact of the structure on the wing weight and stiffness in the context of a preliminary design stage.

B. Description of New MDO Methodology

The distinguishing features of the new MDO methodology presented herein can be summarized as follows:

1) It uses analytical, parameterized representations of wing loads to size the wing structure at every design point, covering the entire range of anticipated loads for the problem at hand
2) The analytical representation of wing loads enables the optimization of the wing structure independently from the

aerodynamic solution, which allows the generation of a set of pre-optimized structures prior to the aerostructural optimization process

3) It employs a surrogate model of the pre-optimized structures, which, among other benefits, facilitates a coupled-adjoint implementation by allowing the rapid evaluation of structural sensitivities via the finite differencing of the surrogate
4) Because the surrogate of the wing structure is generated beforehand, it enables the use of a monolithic architecture for aerostructural optimization, and also eliminates the large number of constraints associated with structural optimization, thus removing the need for the aggregation of constraints in the adjoint method
5) As stated previously, it is well suited for an industrial environment, as the use of pre-generated surrogate models is an effective way of sharing disciplinary tools

1. MDO Architecture

It should be noted that the optimization strategy utilized herein is a variation of the strategy proposed in previous work of the authors [35]. Like the previous architecture, it is a Multidisciplinary Feasible (MDF) [6] method that performs a multidisciplinary analysis (MDA) to converge the wing to static aeroelastic equilibrium at every design cycle, and a surrogate is employed in place of the structural sub-optimization. However, the MDO architecture described in Fontana et al.[35] features two MDA sets, one for converging the aeroelastic deformations under sizing loads, and another for converging the aeroelastic deformations under cruise loads, whereas the work presented herein is a simplified version that requires only one MDA set. This single MDA converges the aeroelastic deformations under cruise loads, while sizing the structure at every design iteration by interrogating the structural surrogate model. To size the structure, the loads provided to the surrogate are the cruise loads multiplied by a set of scaling factors to approximate the spanload resulting from a 2.5g maneuver. These scaling factors were obtained prior to the optimization by running a cruise case and a 2.5g sizing load case for the baseline design and computing the scaling factors at each station along the span that recreate the 2.5g spanload from the 1g spanload.

An eXtended Design Structure Matrix (XDSM) [36] describing this overall process is shown in Figure 1, with its algorithm shown in Algorithm 1. Furthermore, the process used to construct the surrogate model prior to aerostructural optimization is described by the XDSM in Figure 2 and Algorithm 2. As stated previously, the surrogate model represents a structural sub-optimization, i.e. a structural sizing process. It is not necessary to perform CFD simulations to construct the surrogate, as the applied loads are represented analytically, as described in section II.C.

In the present work, this MDO process is carried out by means of several independent codes. The programs are executed in sequence via the SIMULIA Isight process integration framework*, which also enables the automated transfer of data via file I/O. Within this framework, several of the essential functions of this setup, such as the CFD

*SIMULIA Isight. 2018, Dassault Systèmes. https://www.3ds.com/products/simulia/isight

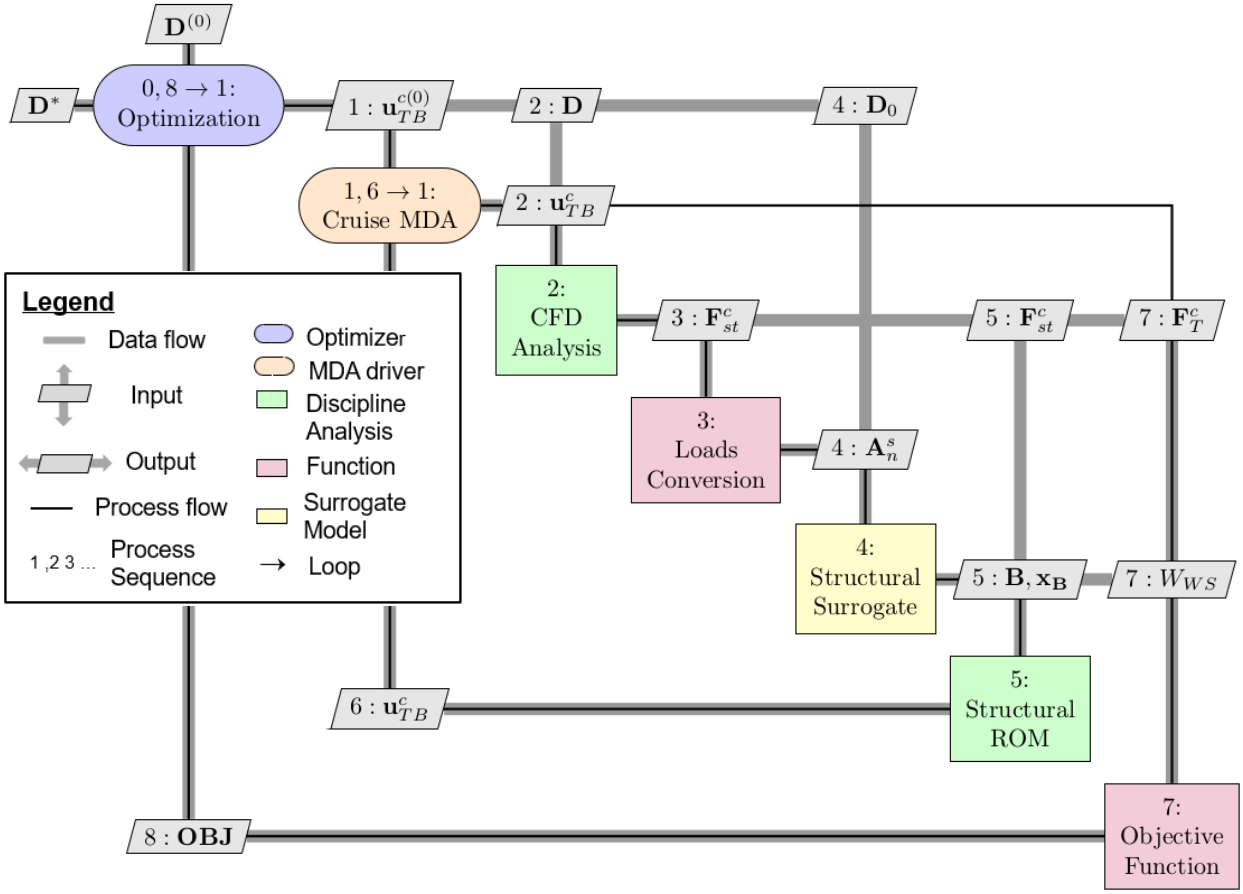

Figure 1 eXtended Design Structure Matrix (XDSM) Diagram of the MDO strategy.

Algorithm 1: Algorithm of the New MDO Method

```
0: Initialize Optimization with baseline design variable values
do
    1: Initialize deflections to 0 for MDA's
    do
        2: Update mesh, based on design changes and deflections, and run CFD Solution
        3: Scale and parameterize resulting aerodynamic cruise loads according to sizing case
        4: Interrogate surrogate, using parameterized sizing loads
        5: Apply cruise loads to structural reduced-order model (ROM) output by the surrogate to obtain
           deflections
        6: Pass deflections to MDA driver to use for next iteration
    until MDA has converged;
    7: Compute objective, performing mission analysis to find fuel weight and compute total A/C weight.
    8: Pass objective value to optimizer to determine next design step
until Optimization has converged;
```

Algorithm 2: Algorithm of the Surrogate Construction

```
0: Initialize DOE with one-shot sampling scheme
do
    1: Initialize structural sub-optimization(sizing)
    do
        2: Generate structural model with planform determined by the DOE and local element thickness
           determined by the sub-optimizer
        3: Apply analytical loads determined by the DOE and obtain structural solution
        4: Compute element stresses from structural solution
        5: Pass stress values to optimizer
    until sub-optimization has converged;
    6: Compute Weight and stiffness of sized wing-structure (create structural ROM)
until For every DOE point;
```

flow solution, are performed by the high-fidelity Reynolds Averaged Navier-Stokes (RANS) solver, NSU3D [37], and its accompanying suite of programs. Specifically, the fluid-structure interface (FSI), mesh deformation tool, and flow-solution post-processor, are all part of the NSU3D program, which includes a collection of fortran modules customized for the present work. The MDO process is decomposed in detail in terms of these and the functions of other codes in Section II.F. It should be noted that the NSU3D suite was chosen for this task in part because of its internal adjoint sensitivity capabilities [38], which are an integral part of the present method, as discussed in Section II.F.

2. Coupled-Adjoint Sensitivity Analysis

Gradient-based optimization techniques greatly reduce the expense of solving large-scale optimization problems, and thus it is desirable for any MDO method to facilitate an efficient computation of the gradients. To this end, the adjoint method provides a means of computing gradients in which the computational cost is virtually independent of the number of design variables. On the other hand, the number of objective and constraint functions do have a significant impact on the cost of the adjoint method, so ideally this number should be kept small, where possible [39, 40].

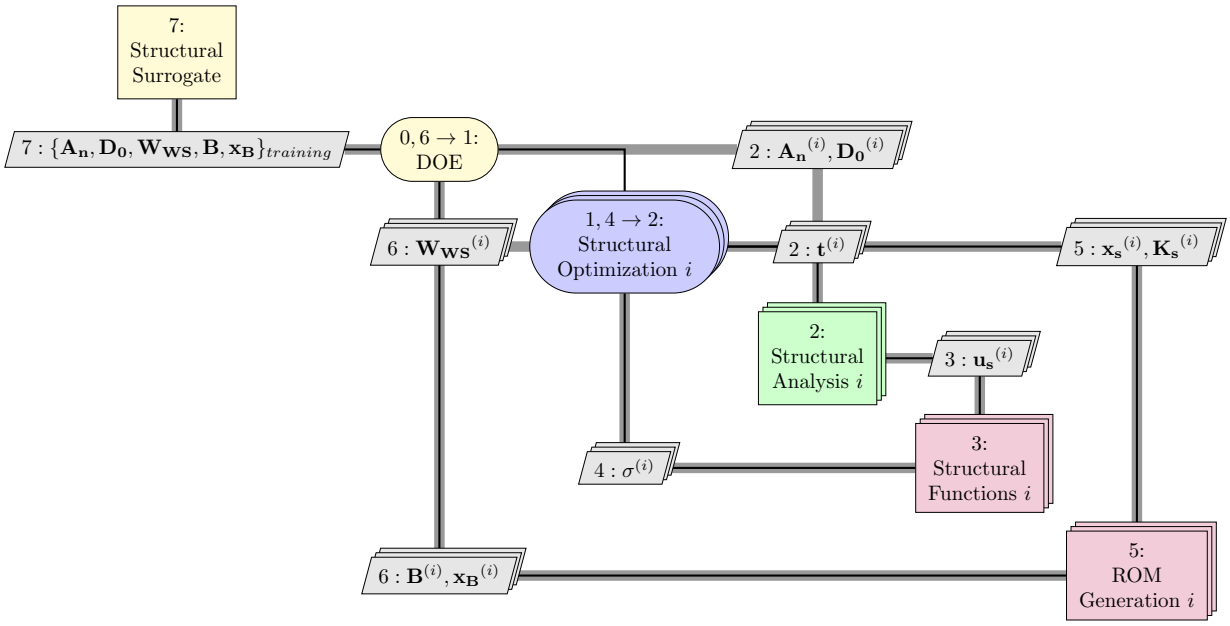

Figure 2 eXtended Design Structure Matrix (XDSM) Diagram of the process used to collect training data for the structural surrogate.

The coupled-adjoint method as described by Martins [41] forms the foundation of the adjoint implementation of the present work. However, the methodology is modified and expanded to adapt it to the new MDO strategy, and is discussed in Section II.F.

C. Loads Parameterization

1. Lift Distribution

The parameterization method chosen for the wing lift distribution is the classic Fourier series method originally developed by Glauert [42]. In this method, the lift distribution is given as

$$\frac{C_l c}{c_{av}} = 4AR \sum_n \bar{A}_n \sin(n\theta), \tag{1}$$

where c_{av} is the average chord, AR is the wing aspect ratio, and $\bar{A}_n$ are the Fourier coefficients. C_l and c are the sectional lift coefficient and the local chord, respectively, as functions of the nondimensional spanwise coordinate θ, which is defined by

$$y = (b/2)\cos(\theta), \tag{2}$$

where b is the wingspan, and y is the dimensional spanwise coordinate, ranging from $-b/2$ to $b/2$.

Further details on the expansion of equation 1 to compute the associated internal shear and bending moment distributions are provided in [35].

2. Pitching Moment Distribution

The pitching moment distribution is modeled in terms of the center-of-pressure chordwise locations at a number of wing spanwise stations. This approach is chosen because it allows the pitching moment to be linked directly to the lift distribution via the center-of-pressure location (assuming the contribution of the drag force is negligible). Therefore, the pitching moment about the quarter-chord at any spanwise station can be written as

$$C_{m,QC} = (0.25 - (x/c)_{cp})C_l, \tag{3}$$

where $(x/c)_{cp}$ is the local center-of-pressure chordwise location. To properly capture the whole spanwise pitching moment distribution, the $(x/c)_{cp}$ values are computed at a number of spanwise locations, and then interpolated with a simple piecewise linear function.

For convenience, the $\bar{A}_n$ and $(x/c)_{cp}$ vectors that define the lift and pitching moment distributions, respectively, and the wing C_L, are concatenated into a single vector, which is denoted as A_n:

$$A_n = (\bar{A}_n, (x/c)_{cp}, C_L) \tag{4}$$

D. Structural Surrogate

1. Inputs and Outputs

As mentioned in Section II.B.1, the structural surrogate model utilized in this work is a substitute for the disciplinary sub-optimization process, returning both the weight and equivalent stiffness of an optimized wing structure. The weight and stiffness of the sized wing structure are influenced by both geometric design variables and the sizing load. In practice, the wing loading consists of three components, namely the lift, drag and pitching moment distributions. To minimize the number of surrogate input parameters, two approximations are employed herein:

1) The drag load influence on the structure is assumed to be negligible.

2) Analytical, parameterized equations are used to model the wing load distribution.

The input and output parameters of the structural model are shown in Table 1, where C_L is the total lift coefficient used to determine the first Fourier coefficient of the wing lift distribution, as discussed in the previous work [35]. $\bar{A}_n$ and $(x/c)_{cp}$ are the Fourier coefficients and spanwise center-of-pressure locations that describe the shape of the lift and pitching moment distributions, respectively, $b/2$ is the semi-span, $\Delta\Lambda_{TE}$ is the change in sweep angle of the trailing

Table 1 Surrogate Inputs and Outputs

Inputs		**Outputs**	
Loads Parameters	Geometry Parameters	Beam Parameters	Weight Parameters
C_L	$b/2$	x_B [3 per bay]	W_{WS}
$\bar{A}_n$ [4 parameters]	$\Delta\Lambda_{TE}$	A [1 per bay]	
$(x/c)_{cp}$ [4 parameters]	$\Lambda_{TE,ibk}$	I_y [1 per bay]	
	(t/c) [$\sim$ 5 variables]	I_z [1 per bay]	
		J [1 per bay]	
Total = $\sim$ 20 **variables**		**Total = (7*nbays) + 1 variables**	

edge at the kink, $\Lambda_{TE,ibk}$ is the trailing-edge sweep inboard of the kink, and (t/c) denotes the wing maximum thickness at several wing spanwise stations. The wing maximum thickness distribution is modeled with 3 to 5 spanwise variables, depending on the wing geometry. The output beam parameters, for each bay, consist of the second moment of area about the z-axis (I_z), the second moment of area about the y-axis (I_y), the polar second moment of area (J), the cross-sectional area (A), and the elastic axis coordinates (x_B), which define the location of the beam elements. These parameters assume an Euler-Bernoulli beam model.

It should be noted that the method as a whole does not preclude the use of different or additional inputs or outputs. Including more geometric inputs could expand the model's applicability to a wider class of aircraft, or including another set of parameterized loads could increase the fidelity of the structural sizing. However, it is advantageous to minimize the number of surrogate inputs to avoid the "curse of dimensionality". For this reason, it is envisioned that parameterized envelope loads may be used to approximate the influence of all load cases in a single set of loads, as discussed in previous work [35].

The number of surrogate outputs, however, is more flexible. A separate surrogate model could be constructed for each output, but the same training data-set could be used for each one. Therefore, the computational cost for training the model scales well with the number of outputs. In light of this, it is envisioned that a more sophisticated structural ROM could be used, such as a Nastran superelement model of the structure [43].

E. Objective and Analysis Functions

In order to form the sensitivity equations, the relationships between the independent and dependent variables of the system need to be defined for both the objective equation and the residual equations. The objective equation consists of a term for the total aircraft weight and a term for a CL-target penalty, with a weighting constant multiplying each,

$$OBJ = \beta_1 W_{A/C} + \beta_2 (C_L^c - C_{L,Target}^c)^2 \tag{5}$$

where the aircraft total weight consists of a fuel weight term and a wing structural weight term, which are updated during the optimization, and a constant weight term, which accounts for the weight of the payload and all other aircraft components:

$$W_{A/C} = (W_{WS} + W_{WS,center})(2.0)(1.25) + W_f + W_{other} \tag{6}$$

The weight of the sized, exposed wing structure, W_{WS}, is computed via the structural surrogate model, which is then added to a constant term for the center wingbox weight, $W_{WS,center}$, multiplied by 2.0 to account for both wings, and multiplied by 1.25 to account for fasteners and other structural details, as was done in Brooks et al. [44].

The fuel weight, on the other hand, is computed via the Breguet range equation for a fixed-range mission,

$$W_f = ((W_{WS} + W_{WS,center})(2.0)(1.25) + W_{other})\left(\exp\left(\frac{Rc_t}{V_\infty(C_L^c/C_D^c)}\right) - 1\right) \tag{7}$$

where R is the aircraft range, V_∞ is the true airspeed, and c_t is the thrust-specific fuel consumption.

Substituting equations 6 and 7 into equation 5, yields,

$$OBJ = \beta_1\left(((W_{WS} + W_{WS,center})(2.0)(1.25) + W_{other})\exp(\frac{Rc_t}{V_\infty(C_L^c/C_D^c)})\right) + \beta_2(C_L^c - C_{L,Target}^c)^2 \tag{8}$$

W_{WS}, C_L, and C_D are the variables in equation 8 that change during the optimization. Therefore, the objective may be considered a function of these variables:

$$OBJ = OBJ(W_{WS}, C_L^c, C_D^c) \tag{9}$$

For simplicity of notation, C_L and C_D are concatenated into a vector of total force coefficients for the cruise case, denoted as F_T^c. Therefore, equation 9 may be rewritten as

$$OBJ = OBJ(W_{WS}, F_T^c) \tag{10}$$

where F_T^c and W_{WS} are obtained from the flow solver and the structural surrogate, respectively. However, the flow solver and structural surrogate are coupled in the MDA solution process. Therefore, it is necessary to describe them in terms

of the entire MDA system. This is described in Table 2, where each important function of a single MDA cycle is listed, showing how each process is a function of the outputs from preceding processes.

D_G is a vector of NSU3D-specific geometric input parameters that describe the wing jig design shape, and take a different form than the overall design variables used in the Isight framework, which are denoted as the vector D. D includes both wing planform and sectional shape design variables. Therefore D_G needs to be computed from D in item 1 of Table 2 before proceeding to the functions of NSU3D, items 3 through 7. The twist and bending deflections resulting from the previous MDA cycle are denoted as $\hat{u}^c_{TB}$. These are used to update the wing surface coordinates, x^c_{sf}, within NSU3D, in conjunction with the design changes obtained through D_G. Once NSU3D moves the mesh (item 4), and computes the flow solution (item 5), sectional aerodynamic force coefficients and chords, F^c_{st}, are extracted from the results, as well as the total force coefficients, F_T. The sectional results are used to compute the parameterized sizing loads, A^s_n, in item 8. For simplicity of notation, the A_n vector listed here includes not only the Fourier coefficients to represent the shape of the spanload, but the total C_L and center-of-pressure parameters as well. The next three items of Table 2, the wing structural weight, W_{WS}, beam stiffness parameters, B, and beam elastic axis coordinates, x_B, are outputs of the structural surrogate and are therefore dependent on A_n. B represents the vector of all beam stiffness parameters,

$$B = \{A, I_y, I_z, J\} \tag{11}$$

The surrogate outputs are also dependent upon several of the Isight geometric design variables listed in Table 1. These are denoted here as the vector D_0, a subset of the Isight design variables, D, that are shared by both the aerodynamic and structural disciplines. Namely, these are the wing thickness and planform variables listed among the surrogate inputs in Table 1. The beam model produced by the surrogate is subject to the sizing loads in discrete form, and then the resulting deflections are interpolated onto the set of sectional wing stations used by NSU3D, producing u_{TB} for the next iteration.

F. Coupled-Adjoint Implementation

In addition to a surrogate model of the sized wing structure, the second main feature of the present approach is that the adjoint method is used to obtain coupled sensitivities, as stated previously. A modified version of the coupled-adjoint approach, adapted to accommodate the presence of the structural surrogate, is presented herein.

1. Tangent Formulation

Once all the relevant functions and variables have been established, the sensitivity equations may be derived. Here, these are derived in their tangent representation before proceeding to the adjoint formulation. The goal is to obtain the gradient of the objective, therefore we take the total derivative of the objective equation, Equation 10, yielding,

Table 2 Functions involved in the MDA process

Item#	Function	Description
1	$D_G(D)$	NSU3D geometric input parameters derived from Isight design variables
2	$\hat{u}^c_{TB}(u^c_{TB})$	Sectional wing deflections used for CFD analysis
3	$x^c_{sf}(D_G, \hat{u}^c_{TB})$	New wing surface coordinates from updated design variables and structural deflections from the previous iteration of the MDA
4	$G^c(x^c, x^c_{sf})$	Mesh deformation residuals
5	$R^c(x^c, \omega^c, D^c_\alpha)$	Flow residuals
6	${F_{st}}^c(x^c, \omega^c, D^c_\alpha)$	Sectional force coefficients at a set of spanwise stations
7	$F^c_T(x^c, \omega^c, D^c_\alpha)$	Total force coefficients
8	$A^s_n(F^c_{st}, D_o)$	Load parameterization for the station force coefficients
9	$W_{WS}(A^s_n, D_o)$	Weight of sized wing structure from the surrogate model
10	$B(A^s_n, D_o)$	Beam parameters for the sized wing structure from the surrogate model
11	$x_B(A^s_n, D_o)$	Beam elastic axis coordinates for the sized wing structure from the surrogate model
12	$F^c_B(F^c_{st}, x_B, D_o)$	Discrete forces to be applied to the beam model from CFD sectional forces
13	$S^c(K(B, x_B), u^c, F^c_B)$	Structural residuals for the beam model
14	$u^c_{TB}(x_B, u^c)$	Beam nodal twist and bending deflections at aerodynamic force stations

$$\frac{dOBJ}{dD} = \frac{\partial OBJ}{\partial W_{WS}}\frac{dW_{WS}}{dD} + \frac{\partial OBJ}{\partial F^c_T}\frac{dF^c_T}{dD} \tag{12}$$

The partial derivatives of the objective with respect to W_{WS} and F_T are computed analytically by differentiating equation 8. The total derivatives, on the other hand, are computed as part of the system of constraint equations formed from Table 2, in which resulting vectors from each of the 14 functions are considered the independent variables of the system.

Taking the total derivative of each function in Table 2 with respect to the Isight design variables, D, yields:

$$\frac{dD_G}{dD} = \frac{\partial D_G}{\partial D} \tag{13}$$

$$\frac{d\hat{u}^c_{TB}}{dD} = \frac{du^c_{TB}}{dD} \tag{14}$$

$$\frac{dx^c_{sf}}{dD} = \frac{\partial x^c_{sf}}{\partial D_G}\frac{dD_G}{dD} + \frac{\partial x^c_{sf}}{\partial u^c_{TB}}\frac{d\hat{u}_{TB}{}^c}{dD} \tag{15}$$

$$\frac{\partial G^c}{\partial x^c_{sf}}\frac{dx^c_{sf}}{dD} + \frac{\partial G^c}{\partial x^c}\frac{dx^c}{dD} = 0 \tag{16}$$

$$\frac{\partial R^c}{\partial x^c}\frac{dx^c}{dD} + \frac{\partial R^c}{\partial \omega^c}\frac{d\omega^c}{dD} + \frac{\partial R^c}{\partial D_\alpha}\frac{dD_\alpha}{dD} = 0 \tag{17}$$

$$\frac{dF^c_{st}}{dD} = \frac{\partial F^c_{st}}{\partial x^c}\frac{dx^c}{dD} + \frac{\partial F^c_{st}}{\partial \omega^c}\frac{d\omega^c}{dD} + \frac{\partial F^c_{st}}{\partial D_\alpha}\frac{dD_\alpha}{dD} \tag{18}$$

$$\frac{dF^c_T}{dD} = \frac{\partial F^c_T}{\partial x^c}\frac{dx^c}{dD} + \frac{\partial F^c_T}{\partial \omega^c}\frac{d\omega^c}{dD} + \frac{\partial F^c_T}{\partial D_\alpha}\frac{dD_\alpha}{dD} \tag{19}$$

$$\frac{dA^s_n}{dD} = \frac{\partial A^s_n}{\partial F^c_{st}}\frac{dF^c_{st}}{dD} + \frac{\partial A^s_n}{\partial D_o}\frac{dD_o}{dD} \tag{20}$$

$$\frac{dW_{WS}}{dD} = \frac{\partial W_{WS}}{\partial A^s_n}\frac{dA^s_n}{dD} + \frac{\partial W_{WS}}{\partial D_o}\frac{dD_o}{dD} \tag{21}$$

$$\frac{dB}{dD} = \frac{\partial B}{\partial A^s_n}\frac{dA^s_n}{dD} + \frac{\partial B}{\partial D_o}\frac{dD_o}{dD} \tag{22}$$

$$\frac{dx_B}{dD} = \frac{\partial x_B}{\partial A^s_n}\frac{dA^s_n}{dD} + \frac{\partial x_B}{\partial D_o}\frac{dD_o}{dD} \tag{23}$$

$$\frac{dF^c_B}{dD} = \frac{\partial F^c_B}{\partial F^c_{st}}\frac{dF^c_{st}}{dD} + \frac{\partial F^c_B}{\partial x_B}\frac{dx_B}{dD} + \frac{\partial F^c_B}{\partial D_o}\frac{dD_o}{dD} \tag{24}$$

$$\frac{\partial S^c}{\partial u^c}\frac{du^c}{dD} + \frac{\partial S^c}{\partial B}\frac{dB}{dD} + \frac{\partial S^c}{\partial x_B}\frac{dx_B}{dD} + \frac{\partial S^c}{\partial F^c_B}\frac{dF^c_B}{dD} = 0 \tag{25}$$

$$\frac{du^c_{TB}}{dD} = \frac{\partial u^c_{TB}}{\partial x_B}\frac{dx_B}{dD} + \frac{\partial u^c_{TB}}{\partial u^c}\frac{du^c}{dD} \tag{26}$$

Arranging equations 13 through 26 into a matrix system yields:

$$
\begin{bmatrix}
I & 0 & 0 & 0 & 0 & 0 & 0 & 0 & 0 & 0 & 0 & 0 & 0 & 0 \\
0 & I & 0 & 0 & 0 & 0 & 0 & 0 & 0 & 0 & 0 & 0 & 0 & -I \\
-\frac{\partial x_{sf}^c}{\partial D_G} & -\frac{\partial x_{sf}^c}{\partial \hat{u}_{TB}^c} & I & 0 & 0 & 0 & 0 & 0 & 0 & 0 & 0 & 0 & 0 & 0 \\
0 & 0 & \frac{\partial G^c}{\partial x_{sf}^c} & \frac{\partial G^c}{\partial x^c} & 0 & 0 & 0 & 0 & 0 & 0 & 0 & 0 & 0 & 0 \\
0 & 0 & 0 & \frac{\partial R^c}{\partial x^c} & \frac{\partial R^c}{\partial \omega^c} & 0 & 0 & 0 & 0 & 0 & 0 & 0 & 0 & 0 \\
0 & 0 & 0 & -\frac{\partial F_{st}^c}{\partial x^c} & -\frac{\partial F_{st}^c}{\partial \omega^c} & I & 0 & 0 & 0 & 0 & 0 & 0 & 0 & 0 \\
0 & 0 & 0 & -\frac{\partial F_T^c}{\partial x^c} & -\frac{\partial F_T^c}{\partial \omega^c} & 0 & I & 0 & 0 & 0 & 0 & 0 & 0 & 0 \\
0 & 0 & 0 & 0 & 0 & -\frac{\partial A_n^s}{\partial F_{st}^c} & 0 & I & 0 & 0 & 0 & 0 & 0 & 0 \\
0 & 0 & 0 & 0 & 0 & 0 & 0 & -\frac{\partial W_{WS}}{\partial A_n^s} & I & 0 & 0 & 0 & 0 & 0 \\
0 & 0 & 0 & 0 & 0 & 0 & 0 & -\frac{\partial B}{\partial A_n^s} & 0 & I & 0 & 0 & 0 & 0 \\
0 & 0 & 0 & 0 & 0 & 0 & 0 & -\frac{\partial x_B}{\partial A_n^s} & 0 & 0 & I & 0 & 0 & 0 \\
0 & 0 & 0 & 0 & 0 & -\frac{\partial F_B^c}{\partial F_{st}^c} & 0 & 0 & 0 & 0 & -\frac{\partial F_B^c}{\partial x_B} & I & 0 & 0 \\
0 & 0 & 0 & 0 & 0 & 0 & 0 & 0 & 0 & \frac{\partial S^c}{\partial B} & \frac{\partial S^c}{\partial x_B} & \frac{\partial S^c}{\partial F_B^c} & \frac{\partial S^c}{\partial u^c} & 0 \\
0 & 0 & 0 & 0 & 0 & 0 & 0 & 0 & 0 & 0 & -\frac{\partial u_{TB}^c}{\partial x_B} & 0 & -\frac{\partial u_{TB}^c}{\partial u^c} & I
\end{bmatrix}
\begin{bmatrix}
\frac{dD_G^c}{dD} \\
\frac{d\hat{u}_{TB}^c}{dD} \\
\frac{dx_{sf}^c}{dD} \\
\frac{dx^c}{dD} \\
\frac{d\omega^c}{dD} \\
\frac{dF_{st}^c}{dD} \\
\frac{dF_T^c}{dD} \\
\frac{dA_n^s}{dD} \\
\frac{dW_{WS}}{dD} \\
\frac{dB}{dD} \\
\frac{dx_B}{dD} \\
\frac{dF_B^c}{dD} \\
\frac{du^c}{dD} \\
\frac{du_{TB}^c}{dD}
\end{bmatrix}
=
\begin{bmatrix}
\frac{\partial D_G}{\partial D} \\
0 \\
0 \\
0 \\
-\frac{\partial R^c}{\partial D_\alpha}\frac{dD_\alpha}{dD} \\
\frac{\partial F_{st}{}^c}{\partial D_\alpha}\frac{dD_\alpha}{dD} \\
\frac{\partial F_T{}^c}{\partial D_\alpha}\frac{dD_\alpha}{dD} \\
\frac{\partial A_n{}^c}{\partial D_o}\frac{dD_o}{dD} \\
\frac{\partial W_{WS}}{\partial D_o}\frac{dD_o}{dD} \\
\frac{\partial B}{\partial D_o}\frac{dD_o}{dD} \\
\frac{\partial x_B}{\partial D_o}\frac{dD_o}{dD} \\
\frac{\partial F_B{}^c}{\partial D_o}\frac{dD_o}{dD} \\
0 \\
0
\end{bmatrix}
\tag{27}
$$

Correspondingly, the objective gradient equation, given in equation 12, may be rewritten in terms of the total derivatives of the independent variables of equations 27, yielding:

$$\frac{dOBJ}{dD} = \begin{bmatrix} 0 & 0 & 0 & 0 & 0 & 0 & \frac{\partial OBJ}{\partial F_T^c} & 0 & \frac{\partial OBJ}{\partial W_{WS}} & 0 & 0 & 0 & 0 & 0 \end{bmatrix} \begin{bmatrix} \frac{dD_G}{dD} \\ \frac{d\hat{u}_{TB}^c}{dD} \\ \frac{dx_{sf}^c}{dD} \\ \frac{dx^c}{dD} \\ \frac{d\omega^c}{dD} \\ \frac{dF_{st}^c}{dD} \\ \frac{dF_T^c}{dD} \\ \frac{dA_n^s}{dD} \\ \frac{dW_{WS}}{dD} \\ \frac{dB}{dD} \\ \frac{dx_B}{dD} \\ \frac{dF_B^c}{dD} \\ \frac{du^c}{dD} \\ \frac{du_{TB}^c}{dD} \end{bmatrix} \tag{28}$$

This tangent system may be solved iteratively as follows, where k is the iteration counter:

$$\frac{d\hat{u}_{TB}^c}{dD}^{(k)} = \frac{du_{TB}^c}{dD}^{(k-1)} \tag{29}$$

$$\frac{dx_{sf}^c}{dD}^{(k)} = \frac{\partial x_{sf}^c}{\partial D_G}\frac{dD_G}{dD} + \frac{\partial x_{sf}^c}{\partial \hat{u}_{TB}^c}\frac{d\hat{u}_{TB}^c}{dD}^{(k)} \tag{30}$$

$$\frac{\partial G^c}{\partial x^c}\frac{dx^c}{dD}^{(k)} = -\frac{\partial G^c}{\partial x_{sf}^c}\frac{dx_{sf}^c}{dD}^{(k)} \tag{31}$$

$$\frac{\partial R^c}{\partial \omega^c}\frac{d\omega^c}{dD}^{(k)} = -\frac{\partial R^c}{\partial x^c}\frac{dx^c}{dD}^{(k)} - \frac{\partial R^c}{\partial D_\alpha}\frac{dD_\alpha}{dD} \tag{32}$$

$$\frac{dF_{st}^c}{dD}^{(k)} = \frac{\partial F_{st}^c}{\partial x^c}\frac{dx^c}{dD}^{(k)} + \frac{\partial F_{st}^c}{\partial \omega^c}\frac{d\omega^c}{dD}^{(k)} + \frac{\partial F_{st}^c}{\partial D_\alpha}\frac{dD_\alpha}{dD} \tag{33}$$

$$\frac{dF_T^c}{dD}^{(k)} = \frac{\partial F_T^c}{\partial x^c}\frac{dx^c}{dD}^{(k)} + \frac{\partial F_T^c}{\partial \omega^c}\frac{d\omega^c}{dD}^{(k)} + \frac{\partial F_T^c}{\partial D_\alpha}\frac{dD_\alpha}{dD} \tag{34}$$

Next, NSU3D outputs the $\frac{dF_{st}^c}{dD}^{(k)}$ matrix, as well as the $\frac{dF_T^c}{dD}^{(k)}$ matrix, and then the following equations are solved outside of NSU3D:

$$\frac{dA_n^s}{dD}^{(k)} = \frac{\partial A_n^s}{\partial F_{st}^c}\frac{dF_{st}^c}{dD}^{(k)} + \frac{\partial A_n^s}{\partial D_o}\frac{dD_o}{dD} \tag{35}$$

$$\frac{dW_{WS}}{dD}^{(k)} = \frac{\partial W_{WS}}{\partial A_n^s}\frac{dA_n^s}{dD}^{(k)} + \frac{\partial W_{WS}}{\partial D_o}\frac{dD_o}{dD} \tag{36}$$

$$\frac{dB}{dD}^{(k)} = \frac{\partial B}{\partial A_n^s}\frac{dA_n^s}{dD}^{(k)} + \frac{\partial B}{\partial D_o}\frac{dD_o}{dD} \tag{37}$$

$$\frac{dx_B}{dD}^{(k)} = \frac{\partial x_B}{\partial A_n^s}\frac{dA_n^s}{dD}^{(k)} + \frac{\partial x_B}{\partial D_o}\frac{dD_o}{dD} \tag{38}$$

$$\frac{dF_B^c}{dD}^{(k)} = \frac{\partial F_B^c}{\partial F_{st}^c}\frac{dF_{st}^c}{dD}^{(k)} + \frac{\partial F_B^c}{\partial x_B}\frac{dx_B}{dD}^{(k)} + \frac{\partial F_B^c}{\partial D_o}\frac{dD_o}{dD} \tag{39}$$

$$\frac{\partial S^c}{\partial u^c}\frac{du^c}{dD}^{(k)} = -\frac{\partial S^c}{\partial F_B^c}\frac{dF_B^c}{dD}^{(k)} - \frac{\partial S^c}{\partial B}\frac{dB}{dD}^{(k)} - \frac{\partial S^c}{\partial x_B}\frac{dx_B}{dD}^{(k)} \tag{40}$$

$$\frac{du_{TB}^c}{dD}^{(k)} = \frac{\partial u_{TB}^c}{\partial x_B}\frac{dx_B}{dD}^{(k)} + \frac{\partial u_{TB}^c}{\partial u^c}\frac{du^c}{dD}^{(k)} \tag{41}$$

Then, once the total derivatives of the independent variables are obtained from the final iteration, the objective gradient is computed from equation 28.

The tangent method for computing sensitivities is presented here because it is more intuitive to formulate and describe than the adjoint method, and furthermore it may be used to derive the adjoint equations. However, the tangent method itself is not used in the optimization architecture. It is only a means for describing its adjoint counterpart which is presented in section II.F.2.

2. Adjoint Formulation

The adjoint system may be formed from equations 27 and 28. The coefficient matrix of the adjoint system is the transpose of the coefficient matrix of the tangent system, and the R.H.S. of the adjoint system is the transpose of the left-multiplying matrix in the objective equation of the tangent system, 28. These manipulations are explicitly described in Chapter 4 in the original coupled-adjoint work of Martins [41] as well as in previous work by one of the authors [2, 45]. Thus, the adjoint system may be written as:

$$
\begin{bmatrix}
I & 0 & -\frac{\partial x^c_{sf}}{\partial D_G} & 0 & 0 & 0 & 0 & 0 & 0 & 0 & 0 & 0 & 0 & 0 \\
0 & I & -\frac{\partial x^c_{sf}}{\partial \hat{u}^c_{TB}} & 0 & 0 & 0 & 0 & 0 & 0 & 0 & 0 & 0 & 0 & 0 \\
0 & 0 & I & \frac{\partial G^c}{\partial x^c_{sf}} & 0 & 0 & 0 & 0 & 0 & 0 & 0 & 0 & 0 & 0 \\
0 & 0 & 0 & \frac{\partial G^c}{\partial x^c} & \frac{\partial R^c}{\partial x^c} & -\frac{\partial F^c_{st}}{\partial x^c} & -\frac{\partial F^c_T}{\partial x^c} & 0 & 0 & 0 & 0 & 0 & 0 & 0 \\
0 & 0 & 0 & 0 & \frac{\partial R^c}{\partial \omega^c} & -\frac{\partial F^c_{st}}{\partial \omega^c} & -\frac{\partial F^c_T}{\partial \omega^c} & 0 & 0 & 0 & 0 & 0 & 0 & 0 \\
0 & 0 & 0 & 0 & 0 & I & 0 & -\frac{\partial A^s_n}{\partial F^c_{st}} & 0 & 0 & 0 & -\frac{\partial F^c_B}{\partial F^c_{st}} & 0 & 0 \\
0 & 0 & 0 & 0 & 0 & 0 & I & 0 & 0 & 0 & 0 & 0 & 0 & 0 \\
0 & 0 & 0 & 0 & 0 & 0 & 0 & I & -\frac{\partial W_{WS}}{\partial A^s_n} & -\frac{\partial B}{\partial A^s_n} & -\frac{\partial x_B}{\partial A^s_n} & 0 & 0 & 0 \\
0 & 0 & 0 & 0 & 0 & 0 & 0 & 0 & I & 0 & 0 & 0 & 0 & 0 \\
0 & 0 & 0 & 0 & 0 & 0 & 0 & 0 & 0 & I & 0 & 0 & \frac{\partial S^c}{\partial B} & 0 \\
0 & 0 & 0 & 0 & 0 & 0 & 0 & 0 & 0 & 0 & I & -\frac{\partial F^c_B}{\partial x_B} & \frac{\partial S^c}{\partial x_B} & -\frac{\partial u^c_{TB}}{\partial x_B} \\
0 & 0 & 0 & 0 & 0 & 0 & 0 & 0 & 0 & 0 & 0 & I & \frac{\partial S^c}{\partial F^c_B} & 0 \\
0 & 0 & 0 & 0 & 0 & 0 & 0 & 0 & 0 & 0 & 0 & 0 & \frac{\partial S^c}{\partial u^c} & -\frac{\partial u^c_{TB}}{\partial u^c} \\
0 & -I & 0 & 0 & 0 & 0 & 0 & 0 & 0 & 0 & 0 & 0 & 0 & I
\end{bmatrix}^*
\begin{bmatrix}
\lambda_{DG} \\
\hat{\lambda}_{u^c_{TB}} \\
\lambda_{x^c_{sf}} \\
\lambda_{x^c} \\
\lambda_{\omega^c} \\
\lambda_{F^c_{st}} \\
\lambda_{F^c_T} \\
\lambda_{A^s_n} \\
\lambda_{W_{WS}} \\
\lambda_B \\
\lambda_{x_B} \\
\lambda_{F^c_B} \\
\lambda_{S^c} \\
\lambda_{u^c_{TB}}
\end{bmatrix}
=
\begin{bmatrix}
0 \\ 0 \\ 0 \\ 0 \\ 0 \\ 0 \\ \frac{\partial OBJ}{\partial F^c_T}^T \\ 0 \\ \frac{\partial OBJ}{\partial W_{WS}}^T \\ 0 \\ 0 \\ 0 \\ 0 \\ 0
\end{bmatrix}
\tag{42}
$$

*Although not shown, all submatrices of the adjoint coefficient matrix are transposed

$$\frac{dOBJ}{dD} = \begin{bmatrix} \lambda_{DG}^T & \hat{\lambda}_{u_{TB}^c}^T & \lambda_{x_{sf}^c}^T & \lambda_{x^c}^T & \lambda_{\omega^c}^T & \lambda_{F_{st}^c}^T & \lambda_{F_T^c}^T & \lambda_{A_n^s}^T & \lambda_{W_{WS}}^T & \lambda_B^T & \lambda_{x_B}^T & \lambda_{F_B^c}^T & \lambda_{S^c}^T & \lambda_{u_{TB}^c}^T \end{bmatrix} \begin{bmatrix} \frac{\partial D_G}{\partial D} \\ 0 \\ 0 \\ 0 \\ -\frac{\partial R^c}{\partial D_\alpha}\frac{dD_\alpha}{dD} \\ \frac{\partial F_{st}{}^c}{\partial D_\alpha}\frac{dD_\alpha}{dD} \\ \frac{\partial F_T{}^c}{\partial D_\alpha}\frac{dD_\alpha}{dD} \\ \frac{\partial A_n^s}{\partial D_o}\frac{dD_o}{dD} \\ \frac{\partial W_{WS}}{\partial D_o}\frac{dD_o}{dD} \\ \frac{\partial B}{\partial D_o}\frac{dD_o}{dD} \\ \frac{\partial x_B}{\partial D_o}\frac{dD_o}{dD} \\ \frac{\partial F_B{}^c}{\partial D_o}\frac{dD_o}{dD} \\ 0 \\ 0 \end{bmatrix} \quad (43)$$

Matrix equation 42 is solved from the bottom up, using an iterative process:

$$\lambda_{u_{TB}^c}^{(k)} = \hat{\lambda}_{u_{TB}^c}^{(k-1)} \tag{44}$$

$$\frac{\partial S^c}{\partial u^c}^T \lambda_{S^c}^{(k)} = \frac{\partial u_{TB}^c}{\partial u^c}^T \lambda_{u_{TB}^c}^{(k)} \tag{45}$$

$$\lambda_{F_B^c}^{(k)} = -\frac{\partial S^c}{\partial F_B^c}^T \lambda_{S^c}^{(k)} \tag{46}$$

$$\lambda_{x_B}^{(k)} = \frac{\partial F_B^c}{\partial x_B}^T \lambda_{F_B^c}^{(k)} - \frac{\partial S^c}{\partial x_B}^T \lambda_{S^c}^{(k)} + \frac{\partial u_{TB}^c}{\partial x_B}^T \lambda_{u_{TB}^c}^{(k)} \tag{47}$$

$$\lambda_B^{(k)} = -\frac{\partial S^c}{\partial B}^T \lambda_{S^c}^{(k)} \tag{48}$$

$$\lambda_{W_{WS}}^{(k)} = \frac{\partial OBJ}{\partial W_{WS}}^T \tag{49}$$

$$\lambda_{A_n^s}^{(k)} = \frac{\partial W_{WS}}{\partial A_n^s}^T \lambda_{W_{WS}}^{(k)} + \frac{\partial B}{\partial A_n^s}^T \lambda_B^{(k)} + \frac{\partial x_B}{\partial A_n^s}^T \lambda_{x_B}^{(k)} \tag{50}$$

$$\lambda_{F_T^c}^{(k)} = \frac{\partial OBJ}{\partial F_T^c}^T \tag{51}$$

$$\lambda_{F_{st}^c}^{(k)} = \frac{\partial A_n^s}{\partial F_{st}^c}^T \lambda_{A_n^s}^{(k)} + \frac{\partial F_B^c}{\partial F_{st}^c}^T \lambda_{F_B^c}^{(k)} \tag{52}$$

Next, $\lambda_{F_{st}}^{(k)}$ and $\lambda_{F_T}^{(k)}$ are passed into NSU3D, which computes the following:

$$\frac{\partial R^c}{\partial \omega^c}^T \lambda_{\omega^c}^{(k)} = \frac{\partial F_{st}^c}{\partial \omega^c}^T \lambda_{F_{st}^c}^{(k)} + \frac{\partial F_T^c}{\partial \omega^c}^T \lambda_{F_T^c}^{(k)} \tag{53}$$

$$\frac{\partial G^c}{\partial x^c}^T \lambda_{x^c}^{(k)} = -\frac{\partial R^c}{\partial x^c}^T \lambda_{\omega^c}^{(k)} + \frac{\partial F_{st}^c}{\partial x^c}^T \lambda_{F_{st}^c}^{(k)} + \frac{\partial F_T^c}{\partial x^c}^T \lambda_{F_T^c}^{(k)} \tag{54}$$

$$\lambda_{x_{sf}^c}^{(k)} = -\frac{\partial G^c}{\partial x_{sf}^c}^T \lambda_{x^c}^{(k)} \tag{55}$$

$$\hat{\lambda}_{u_{TB}^c}^{(k)} = \frac{\partial x_{sf}^c}{\partial \hat{u}_{TB}^c}^T \lambda_{x_{sf}^c}^{(k)} \tag{56}$$

Then $\hat{\lambda}_{u_{TB}^c}$ is output from NSU3D, to be used in Isight on the next iteration. Once the MDA is complete, the following is computed in NSU3D to obtain λ_{DG}.

$$\lambda_{DG} = \frac{\partial x_{sf}^c}{\partial D_G}^T \lambda_{x_{sf}^c}^{(last)} \tag{57}$$

Lastly, the gradient of the objective is computed from equation 43, which is decomposed in the present implementation, such that some terms are computed by NSU3D, and the rest are computed by another code in the Isight workflow:

$$\frac{dOBJ}{dD} = \lambda_{DG}^T \frac{\partial D_G}{\partial D} + \begin{bmatrix} \hat{\lambda}_{u_{TB}^c}^T & \lambda_{x_{sf}^c}^T & \lambda_{x^c}^T \end{bmatrix} \begin{bmatrix} 0 \\ 0 \\ 0 \end{bmatrix} + \underbrace{\begin{bmatrix} \lambda_{\omega^c}^T & \lambda_{F_{st}^c}^T & \lambda_{F_T^c}^T \end{bmatrix} \begin{bmatrix} -\frac{\partial R^c}{\partial D_\alpha} \\ \frac{\partial {F_{st}}^c}{\partial D_\alpha} \\ \frac{\partial {F_T}^c}{\partial D_\alpha} \end{bmatrix}}_{\text{Solve inside NSU3D. Let this be } \lambda_{D\alpha}^T} \frac{dD_\alpha}{dD}$$

$$+ \begin{bmatrix} \lambda_{A_n^s}^T & \lambda_{W_{WS}}^T & \lambda_B^T & \lambda_{x_B}^T & \lambda_{F_B^c}^T & \lambda_{S^c}^T & \lambda_{u_{TB}^c}^T \end{bmatrix} \begin{bmatrix} \frac{\partial A_n^s}{\partial D_o} \frac{dD_o}{dD} \\ \frac{\partial W_{WS}}{\partial D_o} \frac{dD_o}{dD} \\ \frac{\partial B}{\partial D_o} \frac{dD_o}{dD} \\ \frac{\partial x_B}{\partial D_o} \frac{dD_o}{dD} \\ \frac{\partial {F_B}^c}{\partial D_o} \frac{dD_o}{dD} \\ 0 \\ 0 \end{bmatrix} \tag{58}$$

G. Partial Derivative Details

In order to solve the adjoint equations, the partial derivative terms in Equations 44 through 58 must be computed. The use of a structural surrogate model facilitates this, as the partial derivatives of any surrogate output with respect to any surrogate input may be computed by finite-differencing the computationally inexpensive model. Therefore, this is the means used to compute the partial derivatives of W_{WS}, B, and x_B. Some of the other partial derivative terms are internal to the NSU3D code, and therefore are not discussed here. The remaining partial derivatives are computed analytically, including the partial derivatives of the structural residuals, S, which are determined from the linear elastic structural model as

$$S^c = K(B, x_B)u^c - F_B^c \tag{59}$$

$$\frac{\partial S^c}{\partial u^c} = K \tag{60}$$

$$\frac{\partial S^c}{\partial B} = \frac{\partial K}{\partial B} u^c \tag{61}$$

$$\frac{\partial S^c}{\partial x_B} = \frac{\partial K}{\partial x_B} u^c \tag{62}$$

$$\frac{\partial S^c}{\partial F_B^c} = -I \tag{63}$$

where the derivatives $\frac{\partial K}{\partial B}$ and $\frac{\partial K}{\partial x_B}$ are computed by analytically differentiating the known stiffness matrix formulation for Euler-Bernoulli beam elements.

III. Implementation

A. Aerostructural Workflow

As mentioned previously, the MDO methodology developed herein has been implemented in an Isight workflow . For the CFD solution, mesh movement, and solution of the adjoint equations, the NSU3D Reynolds-Averaged Navier-Stokes code [37, 46] is used. For the wing structural sizing and analysis, a proprietary code from Bombardier Aviation, called S4Wing [47], is used, in conjunction with the Altair OptiStruct structural solver[†]. S4Wing is a smeared-skin wingbox model generator which can also iteratively size the structural elements to achieve a target stress criteria. The target stress settings may be used to calibrate the model to a higher-fidelity structure.

An earlier version of this aerostructural workflow, featuring the aforementioned software, is described in detail in Fontana et al. [35]. The present work expands upon this workflow, which may be run in several different modes. The two main run modes of the workflow are: one to collect training data for the surrogate model, and another to conduct the aerostructural optimization.

When surrogate training data is being collected, NSU3D is not used. A structural model is generated by S4Wing based on the shared geometric design variables. At this stage, the wing spanwise maximum t/c distribution, along with the spanwise distribution of the front and rear spar thicknesses, are used to determine the effective wingbox height at every station. Next, analytical loads are applied to the model, and the structural solution is computed by the Altair OptiStruct code. An iterative structural sizing is conducted by S4Wing, working in tandem with the OptiStruct solver. After the structural sizing, a beam model of the S4Wing structure is created using a method based on the work of Elsayed et al. [48]. An example skin thickness distribution of a sized S4Wing structural model and its corresponding elastic axis used for the equivalent beam is shown in figure 3.

Once the training data is collected, Isight's Approximation component is used to read-in the training data and build the surrogate itself. In addition, an external executable plugin was created so that several techniques from the open-source Surrogate Modeling Toolbox (SMT) [49] may also be used within the Isight framework.

When the aerostructural optimization is being conducted, NSU3D is used for CFD analysis, and S4Wing and Optistruct are not used. The surrogate model acts in place of these structural codes, and the surrogate is interrogated with the aerodynamic loads computed by NSU3D, which are parameterized using the same analytical load function used to build the surrogate. These loads are scaled up to mimic a 2.5g load case before being used in this way. The surrogate then outputs both the weight and stiffness of the sized wing structure. As mentioned previously, after the wing

[†]*OptiStruct. 2021.2. Altair.* https://2021.help.altair.com/2021.2/hwsolvers/os/topics/getting_started/overview_os_r.htm

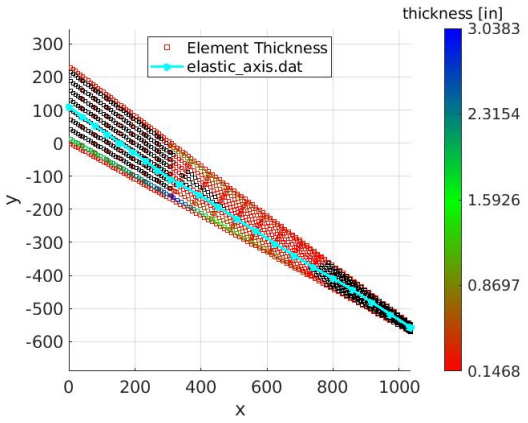

Figure 3 S4Wing structural model element thickness after structural sizing, and corresponding elastic axis used for the equivalent beam model.

structure has been sized, its stiffness properties are captured by means of an equivalent beam model. The output beam parameters and elastic axis coordinates are subsequently used to construct the beam stiffness matrix via an in-house code. Cruise loads are applied to the beam model and structural deflections are obtained using a direct solve of the linear elastic system. Analytical derivatives have been implemented at every stage of the Isight process, except for the derivatives of the surrogate model, which are obtained using finite differences, and the derivatives already available in the NSU3D adjoint implementation. NSU3D has been modified to work in conjunction with the Isight workflow to solve the adjoint system and compute the final objective gradient. All partial derivatives are computed at the final state of the wing in static equilibrium, at the conclusion of the multidisciplinary analysis, and then the iterative process described in II.F is employed to solve for the adjoint vectors and function gradients. The design variables, objective and constraint values are scaled to ensure their magnitudes are all of order 1.0. before being passed to the optimizer, and the gradients are scaled accordingly.

B. Surrogate of Wing Structural Weight and Stiffness

Using the described Isight workflow in the first mode of operation, a series of surrogate models were constructed. In all cases, the training data was collected using Optimal Latin Hypercube (OLH) sampling, for which the input parameters presented in Table 1 were the varying factors. However, the planform parameters and the root t/c parameter were omitted in this study, since the optimization results presented herein are for a fixed-wing-planform optimization. All other inputs and outputs listed in Table 1 were included. Therefore, the surrogate model described herein consists of 13 inputs and 148 outputs.

Previous work of the authors investigated several surrogate modeling techniques to approximate the wing structural weight based on a 2000-point dataset, and the combination of OLH sampling with Elliptical basis function (EBF) modeling was found to be effective [35]. The present work builds upon this by using an EBF model, but beam parameters are also included as surrogate outputs to characterize the stiffness of the structure. Furthermore, several training sets of

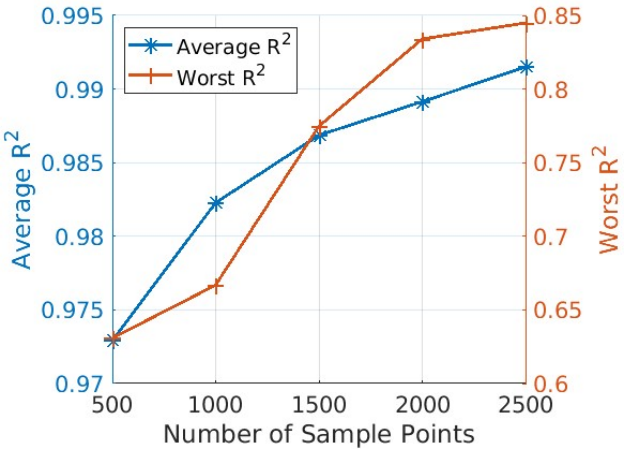

Figure 4 Average and Worst R^2 among all outputs for EBF model built on datasets of various sizes.

different sizes were tested, in order to investigate the influence of the number of sample points on surrogate accuracy. In all cases, a 200-point cross-validation error analysis was conducted to evaluate the model's fit for each of the outputs. Figure 4 shows the average and worst coefficient of determination, R^2, across all 148 outputs as a function of the number of sample points. It is clear that the model's accuracy improves with additional sample points, as expected, with the 2500-point dataset achieving an average R^2 value greater than 0.99. As a further assessment, the number of outputs with R^2 values of various magnitudes, as functions of the number of sample points, are presented in figure 5. As shown, for sample sizes of 1500, 2000 and 2500, only 2 of the 148 outputs have R^2 values less than 0.9, while the vast majority have values greater than 0.99. An EBF model built on 2500 points was therefore selected, as it provided sufficient accuracy. Correlation plots and R^2 values for a sample of the individual outputs for this model are displayed in figure 6. The R^2 for the wing structural weight is slightly greater than it was for the surrogate constructed for previous work [35].

Surrogate models using the Kriging method from the Surrogate Modeling Toolbox package were also investigated. The accuracy of these models was comparable to Isight's EBF, but an additional computational overhead was incurred when running SMT as an external plugin from within the Isight framework. Therefore, it was decided to use EBF for efficiency and ease of use, as the technique is native to the Isight framework.

As mentioned previously, the surrogate is not only used to obtain the weight and stiffness of the sized wing structure, but also the derivatives of those quantities with respect to the surrogate inputs. In the present work, this is done via finite-differencing. Therefore, the accuracy of these finite-difference derivatives must also be assessed. To do this, analytical derivatives of the surrogate model were computed manually, based on the algebraic description of the elliptical basis function technique given in the Isight software documentation[‡], which uses the technique of Mak and Li [50]. In this way, the exact partial derivatives of all outputs with respect to all inputs were obtained at three arbitrary test points in the input space, and the results were compared with those obtained via finite-differencing. Figure 7 shows the

[‡]Dassault Systèmes SIMULIA Isight Component Guide, 2018. "RBF and EBF Models".

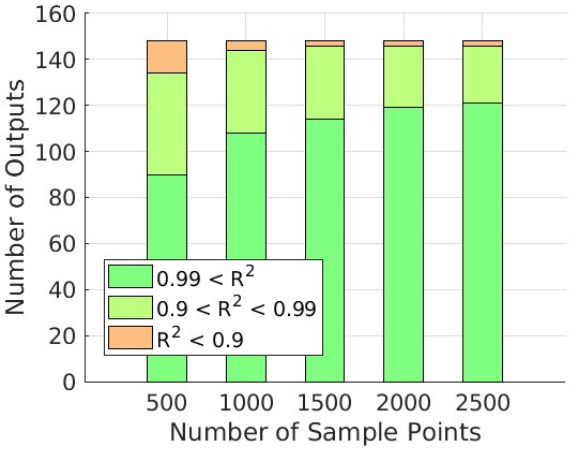

Figure 5 Number of outputs with different levels of R^2 for EBF model built on datasets of various sizes.

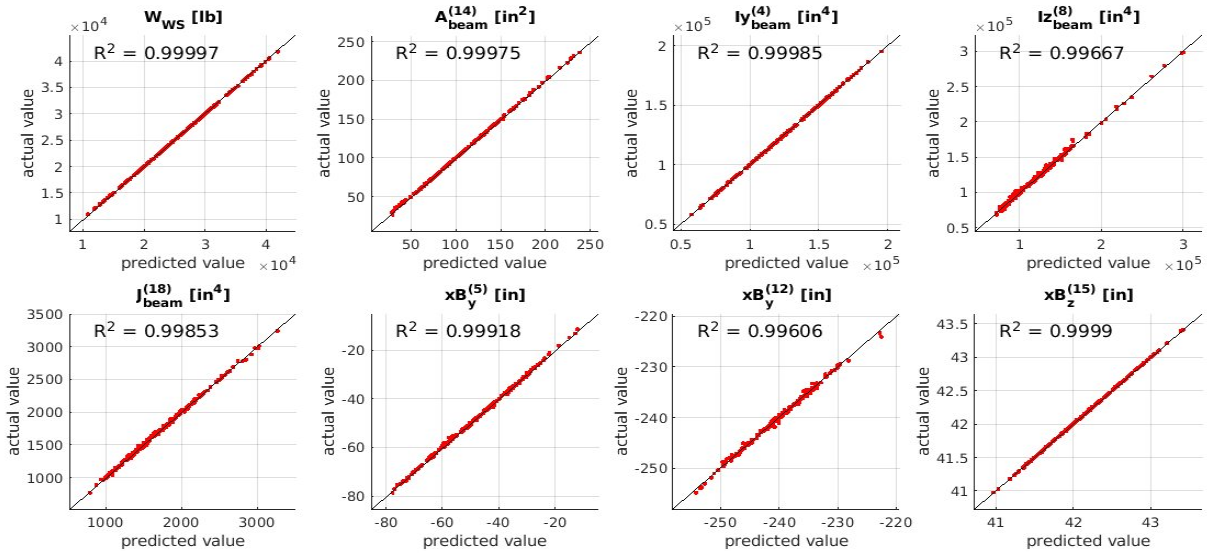

Figure 6 Correlation plots for a sample of surrogate outputs from the 200-point cross-validation of the EBF surrogate model built on the 2500-point dataset.

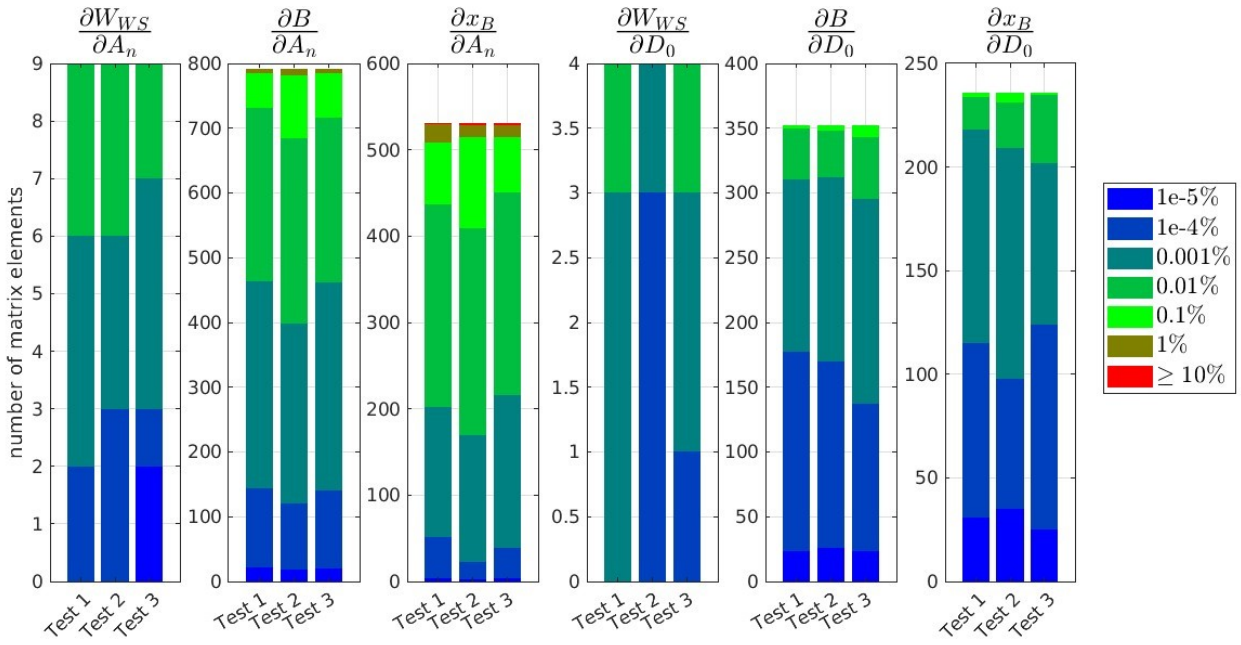

Figure 7 Number of matrix elements having a percent-error level that falls within a given order of magnitude, comparing finite-difference and analytical derivatives at three arbitrary points in surrogate input space.

number of elements in each of the partial derivative matrices that have a percent-error level, relative to the analytical derivatives, that falls within a given order of magnitude. The vast majority of the derivatives have errors of order of 0.01% or less. The very few derivatives that have an error greater than 10% are very small in magnitude compared to the other derivatives of the same matrix.

In addition to comparing against analytical derivatives, the surrogate was examined for smoothness, and the finite-difference derivatives computed with various step sizes were also compared. A series of tests were conducted in which one of the inputs was varied throughout the whole range of the surrogate bounds for that variable, and the surrogate model was interrogated at those points, while the other input variables were left at their values for the initial design of the optimization at static equilibrium. Figure 8 shows the variation of some of the output variables as an input variable changed. The plots also show the finite-difference derivative of the output variable with respect to that input variable for two different step sizes. From plots such as these, we observe that the design space is smooth, and that the computed derivatives do not vary greatly with step size, even if the step size is changed by two or three orders of magnitude. This test, combined with the comparison against analytical derivatives, suggest that the use of finite-differences to compute the surrogate partial derivatives is justified for this application. The advantage of using finite-differences rather than analytical derivatives, in a practical implementation, is that the optimization process is agnostic to the type of surrogate modeling technique used.

The accuracy of the surrogate model presented herein indicates that the methodology can easily be expanded to incorporate a more sophisticated reduced-order model (ROM) of the structure, in lieu of a beam model, if required.

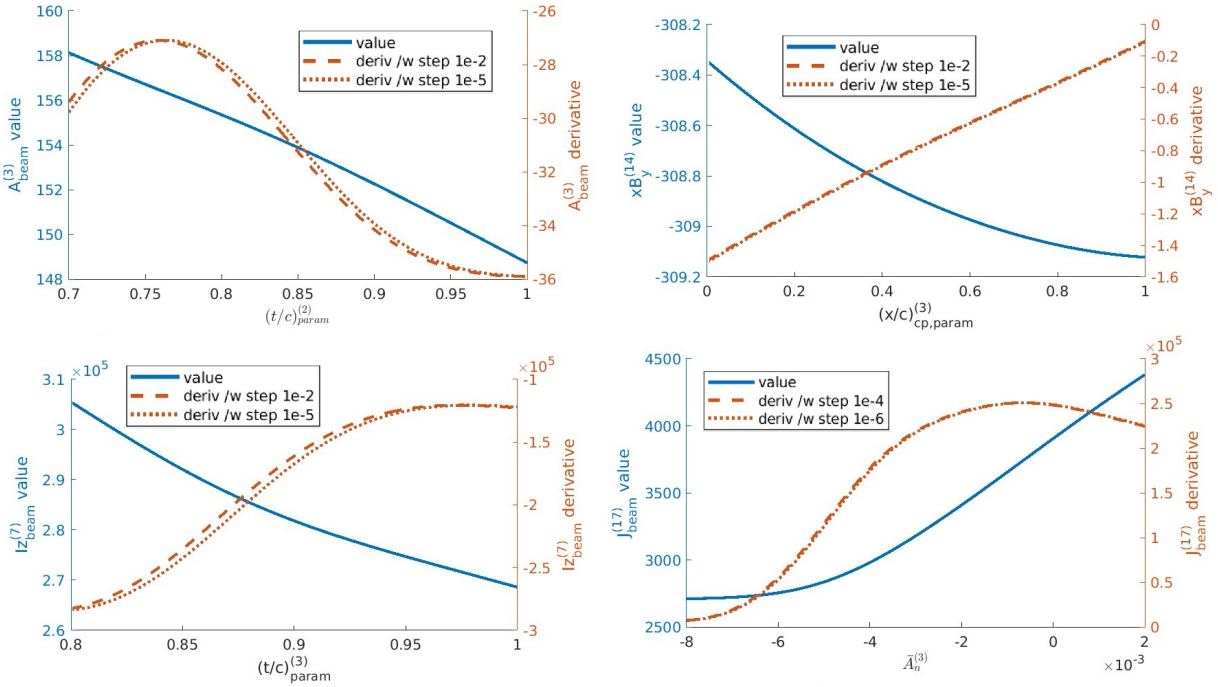

Figure 8 Sample plots of surrogate trends, showing smoothness and consistency of finite-difference derivatives.

This is because the EBF method training cost scales well with the number of outputs, as it only entails solving the same linear system for additional right-hand side vectors[§]. A more sophisticated structural ROM, such as a Nastran superelement model [43], would require a significantly larger number of surrogate outputs, but it may be essential to properly model highly flexible or otherwise unconventional wings.

C. Validation of System-Level Derivatives

It is essential that the accuracy of the system-level derivatives be verified, and the complex-step method is the most accurate means of doing so. To this end, the derivatives computed within NSU3D's adjoint implementation have been previously validated using the complex-step method [51], which showed agreement of the sensitivities to machine precision. Furthermore, the derivatives of the individual components of the Isight workflow were computed by analytically differentiating the embedded codes. However, due to the complexity of the tool chain used in the present work, and the use of Isight as the process integration framework, it was not feasible at this time to implement the complex-step method throughout the entire workflow. Therefore, real-valued finite-differences were used to assess the accuracy of the system-level sensitivities.

After verifying the sensitivities of the individual components of the aerostructural optimization process, a finite-difference test of the entire framework was conducted to verify the sensitivities passed on to the optimizer. This was done at the initial design point of the optimization presented in section IV.

[§]See Dassault Systèmes SIMULIA Isight Component Guide, 2018. "RBF and EBF Models"

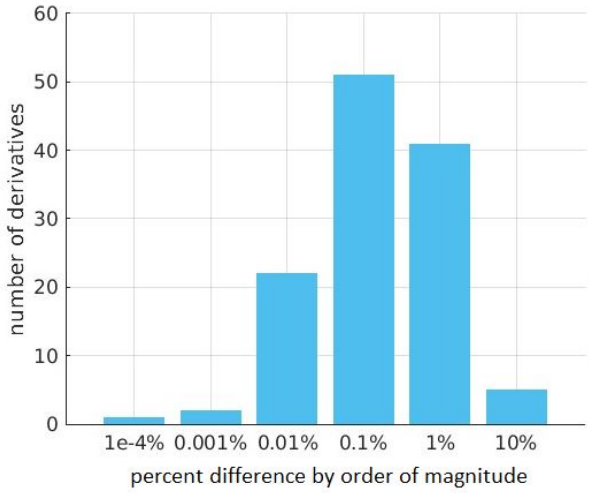

Figure 9 Results of the coupled system derivatives finite-difference test: percent difference levels categorized by order of magnitude.

The percent differences between the gradients obtained with finite-differencing and the gradients obtained via the adjoint process of section II.F were compared, and the results categorized in terms of the order of magnitude of the percent error. Figure 9 presents the number of elements in the gradient vector that have a percent error difference within each order of magnitude. Generally, it was found that derivatives with larger percent errors were typically smaller in magnitude than those with smaller percent errors. Different step sizes were also investigated during the finite-difference tests, using step sizes of 1e-5, 1e-6, 1e-7, as well as a central difference test with a step of 1e-5. However, it was found that the overall correlation of the derivatives did not improve significantly as the finite-difference step sizes were reduced further. Nevertheless, as shown in figure 9, it was found that out of the 122 derivatives, the vast majority show a percent difference of order of 1% or less. These results, together with the successful aerostructural optimization of the CRM wing presented in section IV, speak to the overall accuracy of the derivatives.

IV. Results

The new methodology was applied to a fixed-wing-planform, aerostructural optimization of the CRM configuration. A wing-body-tail mesh of this configuration is shown in Figure 10. Since the CRM mesh is originally in the 1-g flight shape, a wing jig twist and dihedral needed to be computed, such that the original CRM flight twist is reproduced when an optimized wing structure for the CRM is subjected to the 1-g cruise load case. This type of procedure has been performed by several other researchers [14, 52–54], and a similar procedure was performed for this work.

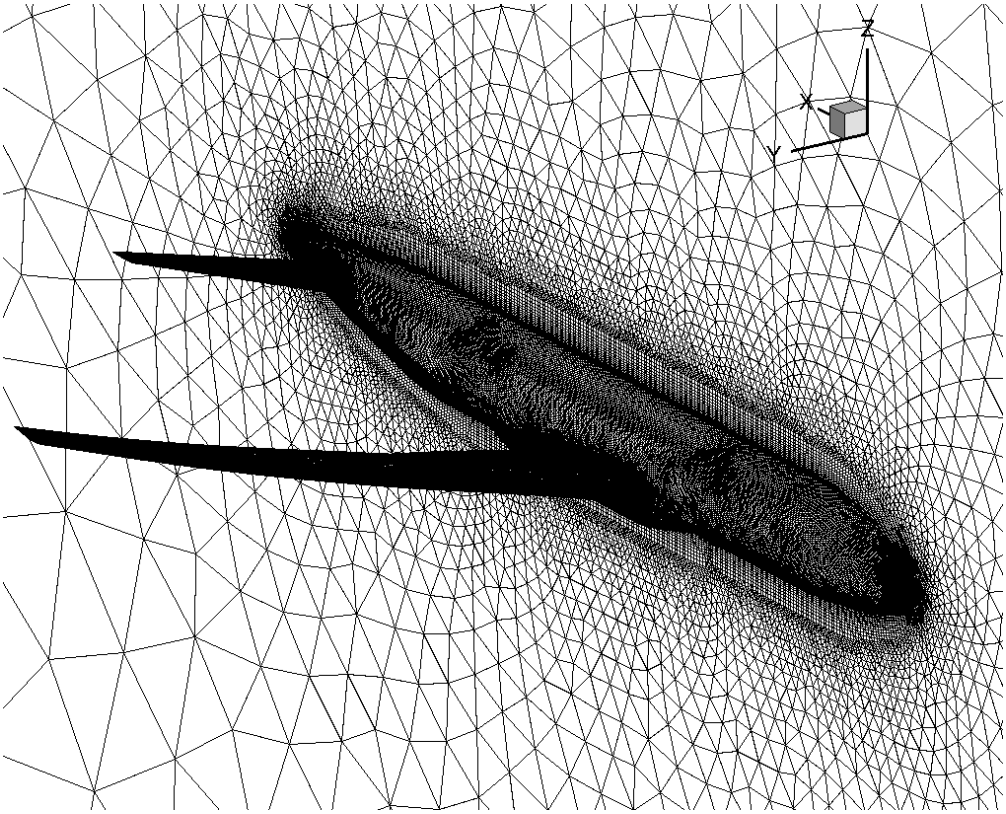

Figure 10 CRM "v3-medfine" wing-body-tail mesh.

The objective of the optimization is given by equation 5. A target lift coefficient of 0.5 was enforced as part of the objective, and the gradient-based optimization algorithm used was SNOPT [55].

The values used for the weighting coefficients of the objective function, β_1 and β_2, were 0.0001 and 1000.0, respectively. These were chosen so that both terms are of similar magnitude. The Breguet range equation (7) and equation 6 were used to compute the total aircraft weight based on the configuration L/D computed using NSU3D, and the wing structural weight, W_{WS}, was obtained from the structural surrogate. The weight of the remaining components of the aircraft was based on the work of Brooks et al. [56].Specifically, W_{other} included the reserve fuel weight, fixed weight, and payload weight, totalling 359,353 lb. The constant center wingbox weight, $W_{WS,center}$, was obtained from the publicly available Undeflected Common Research Model (uCRM) of Brooks et al. [44], amounting to 6586 lb for one wing. The uCRM was also used as a reference to apply static point loads to the wing structure of this work. These static loads accounted for the nominal fuel weight, leading-edge and trailing-edge weight, and engine weight. The weight of the wing structure itself was applied in the same manner, as a static load independent of the structural sizing. All of these point loads were applied to the beam model during the optimization, and also to the S4Wing model during the construction of the surrogate.

The aerodynamic mesh used in this work was a publicly available wing-body-tail mesh of the CRM configuration

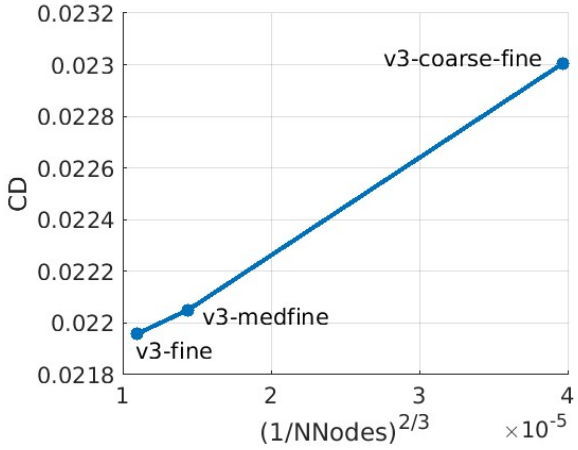

Figure 11 Comparison of C_D for three different CRM wing-body-tail meshes of different refinement.

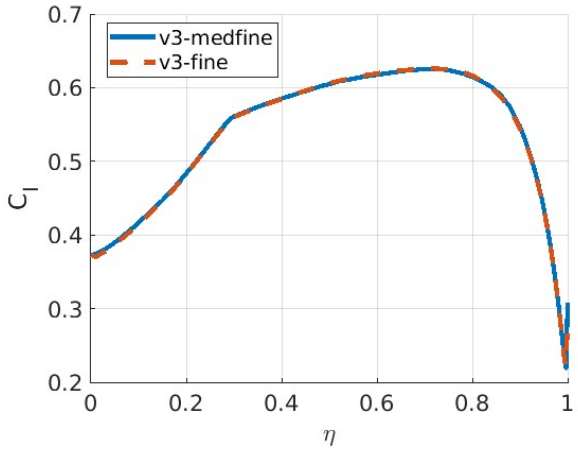

Figure 12 Comparison of C_l distributions for two CRM wing-body-tail meshes of different refinement.

from the Fourth AIAA Drag Prediction Workshop (DPW) [57]. In order to determine which mesh had sufficient refinement for this application, the CFD results from several meshes in their original flight shape were compared at the standard CRM design conditions of Mach=0.85, CL=0.5, and Re= 43M. Figure 11 compares the C_D values obtained from the "v3-coarse-fine", "v3-medfine" and "v3-fine" Boeing unstructured "Best Practices" meshes[¶] of the aforementioned workshop vs the number of nodes of each mesh raised to the power of negative two-thirds. The C_D is seen to converge toward the mesh-independent value as more refined meshes are used.

The number of nodes for these three meshes are 4 million, 18.2 million, and 27.4 million. As an additional check, the C_l and C_m distributions of the "medfine" and "fine" meshes were compared, shown in figures 12 and 13.

One may observe from figures 11, 12, and 13 that the "v3-fine" and "v3-medfine" mesh are close in drag value and nearly identical in terms of sectional C_l and C_m distributions. Furthermore, their wing pressure distributions are almost

[¶]"Index of DPW4". *NASA*.https://dpw.larc.nasa.gov/DPW4/unstructured_Boeing_STL/BEST_PRACTICE_GRIDS/

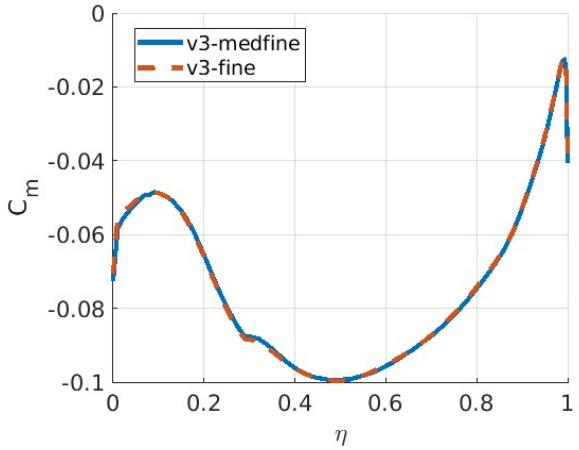

Figure 13 Comparison of C_m distributions for two CRM wing-body-tail meshes of different refinement.

identical as well, as shown in figure 14.

Given these results, the "v3-medfine" mesh was chosen for the optimization, in order to maintain sufficient accuracy without excessive computational cost. It was also verified that the "v3-medfine" mesh featured a y+ value less than 1.0 everywhere on the wing surface at the standard CRM flight condition. The mesh is shown in Figure 10.

To compute the lift-to-drag ratio of the configuration, a correction of 35 drag counts was added to the drag from the CFD analysis to compensate for the missing nacelle, pylon andvertical tail. The standard CRM design conditions of Mach=0.85, CL=0.5, and Re= 43M were used as the cruise condition for this optimization. The cruise wing spanload was multiplied by a set of spanwise scale factors to obtain the wing spanload of the sizing case, which was used to interrogate the structural surrogate, as described in Section II.B.1. For this case, the scale factors mapped the loads at nominal cruise conditions to those at Mach=0.64, Lift=2.5MTOW, at sea level, to simulate a 2.5g symmetric pull-up maneuver.

The surrogate of the wing structure was built using the Elliptical Basis Function (EBF) technique available in the Isight process integration framework, as described in Section III.B.

The optimization used 122 design variables, consisting of 28 airfoil shape parameters at each of 4 airfoil stations, 5 twist parameters, 4 thickness parameters, and one parameter for the angle of attack. The airfoil shape parameters consisted of 14 Hicks-Henne bump functions [58] for the upper surface, and 14 for the lower surface of each airfoil. Eight geometric constraints were also employed, to enforce a minimum ratio of airfoil front and rear spar thicknesses relative to the local airfoil maximum thickness. This was done to ensure that the optimizer did not carve out the airfoils at the spar locations to produce unrealistic shapes. The design variables and constraints are summarized in Figure 15.

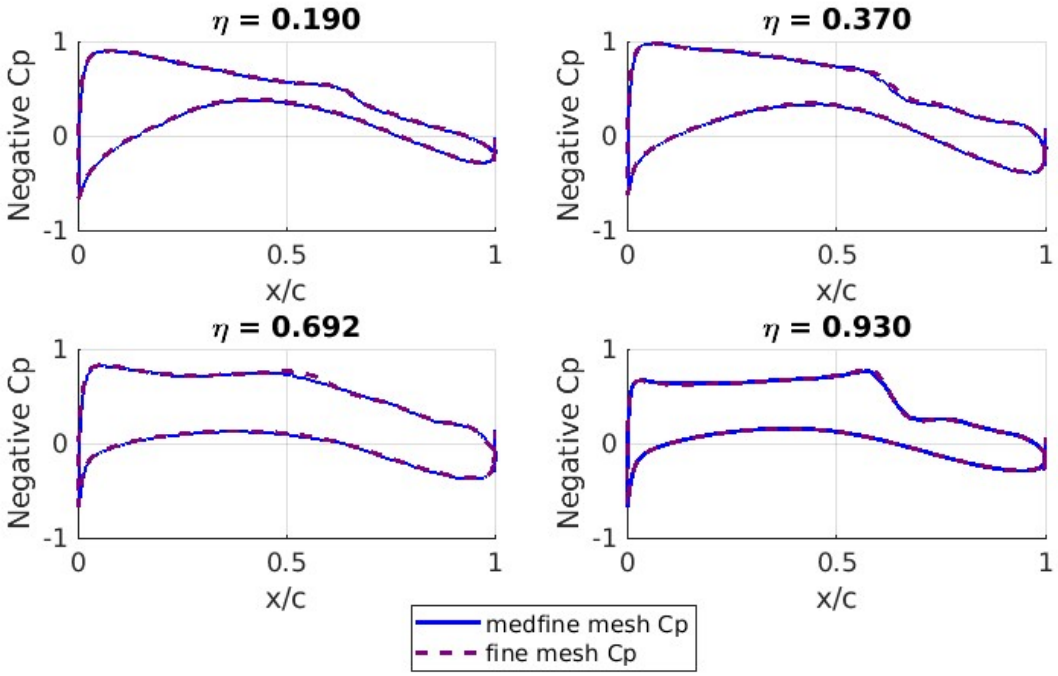

Figure 14 Slices of cp at four spanwise stations for v3-medfine and v3-fine meshes.

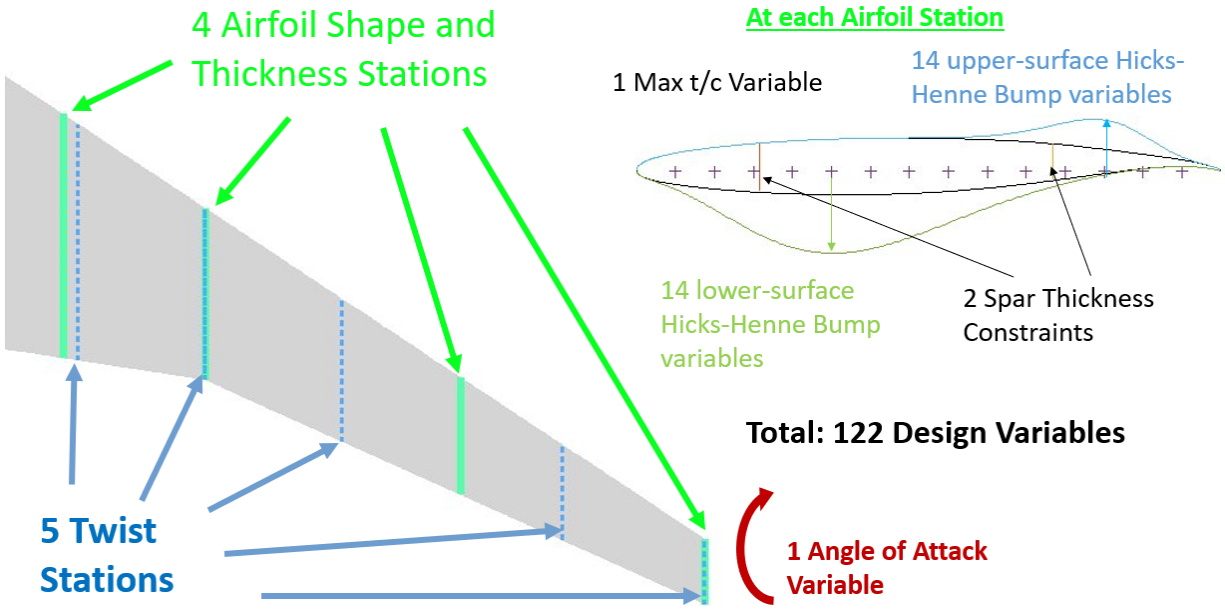

Figure 15 Design variables and constraints used for the aerostructural optimization.

The results of the optimization are shown in Figures 16 to 23.

After 87 iterations, the optimizer reduced the objective by 2.23%, as shown in the objective history in figure 16.

To achieve this, it decreased the required fuel weight, decreased the structural weight, and brought the C_L closer to the C_L target. Figure 16 shows the changes in fuel burn weight W_f and wing structure weight W_{WS} for every objective-improving design. The initial fuel burn and structure weight were 228,384 lb and 19,778 lb, respectively, where the wing structure weight discussed here is strictly W_{WS}, as it is the weight of one wing structure, excluding the center wingbox weight and the 1.25 factor shown in equations 6 - 8.

Figure 16 shows that the optimizer reduced the required fuel weight by 5909 lb, and decreased the structural weight by 3196 lb. Recall that the design variables that are local to the structural discipline are optimal for every iteration, since the surrogate model represents a structural sizing process. Therefore, the reduction in structural weight is only due to aerodynamic load changes and wing thickness changes for this fixed-planform optimization.

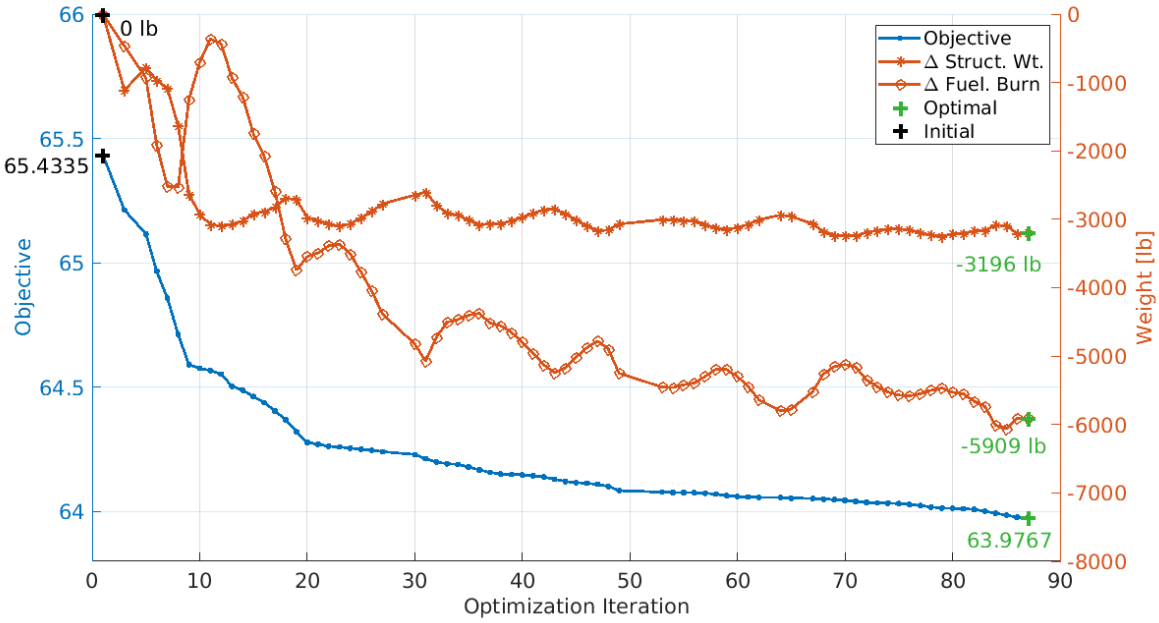

Figure 16 Objective, fuel burn change, and structural weight change history for objective-improving designs.

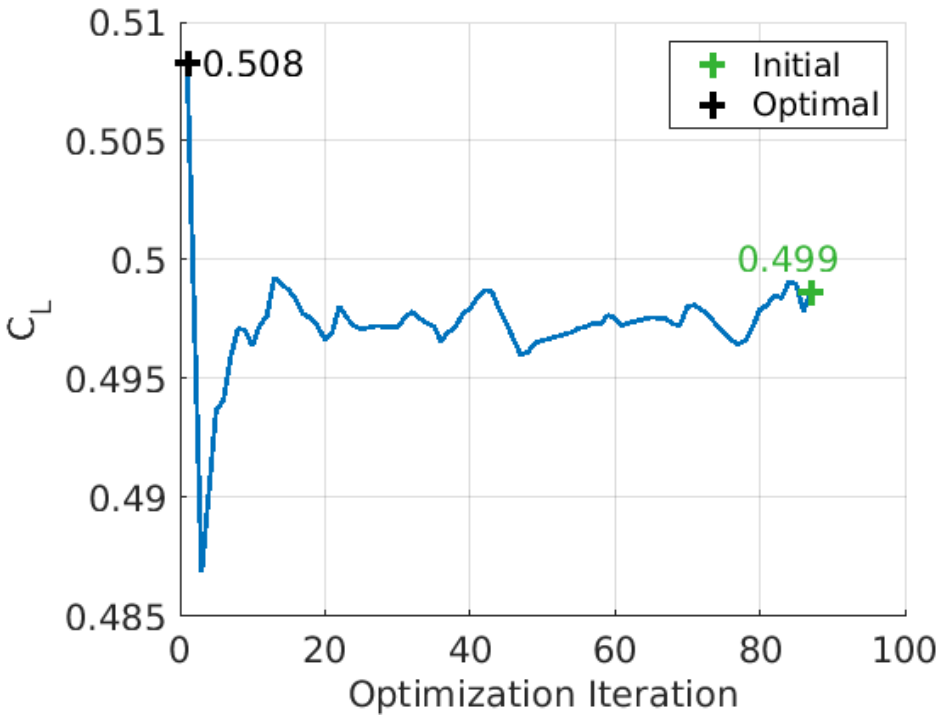

Figure 17 History of total CL at objective-improving designs.

Figure 18 shows that the spanload shifted inboard from its initial position, reducing bending moment on the structure. This is in part due to the more negative jig twist, which can be seen in figure 19. At the same time, the wing thickness decreased everywhere along the span, as shown in figure 20, which incurs a penalty to structural weight, but improves the aerodynamics. The wing thickness was not at the lower bound, however, suggesting that the aerodynamic benefits were balanced by this structural weight penalty.

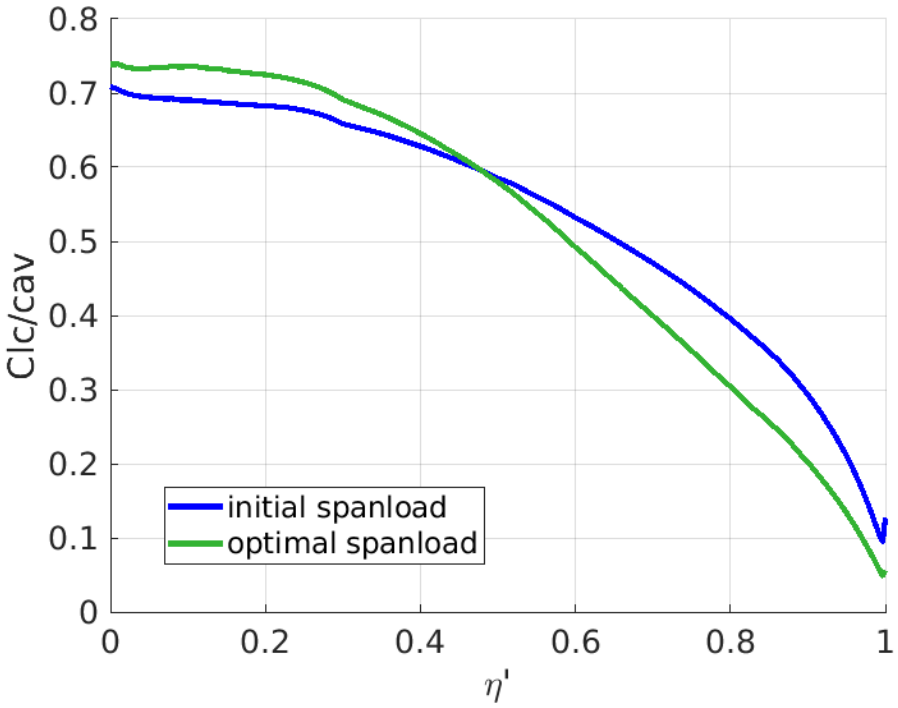

Figure 18 Wing spanload comparison between initial and optimal designs.

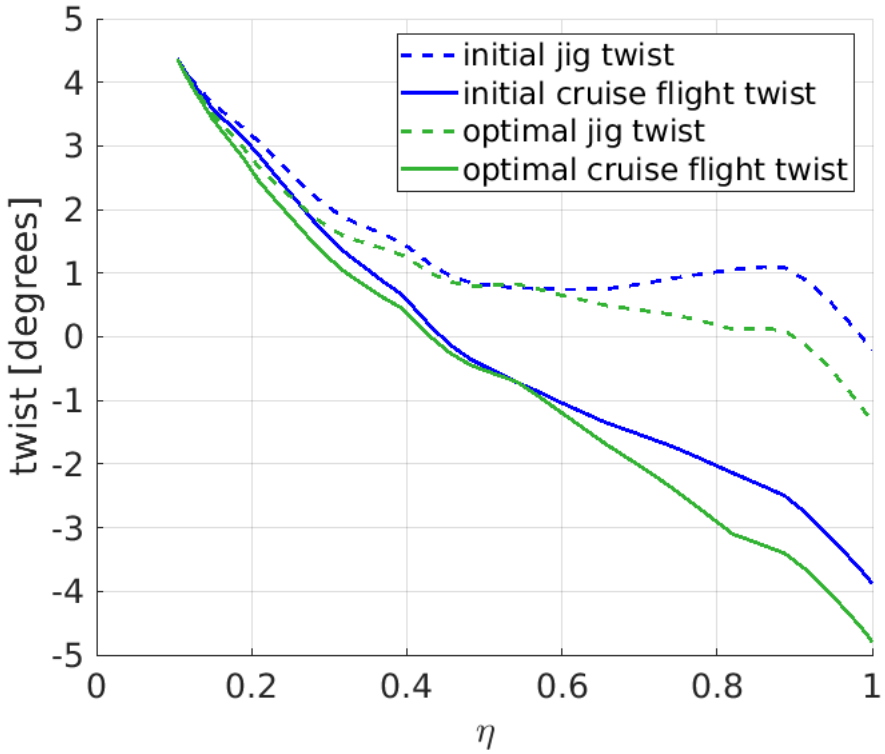

Figure 19 Wing twist distribution comparison between initial and optimal designs.

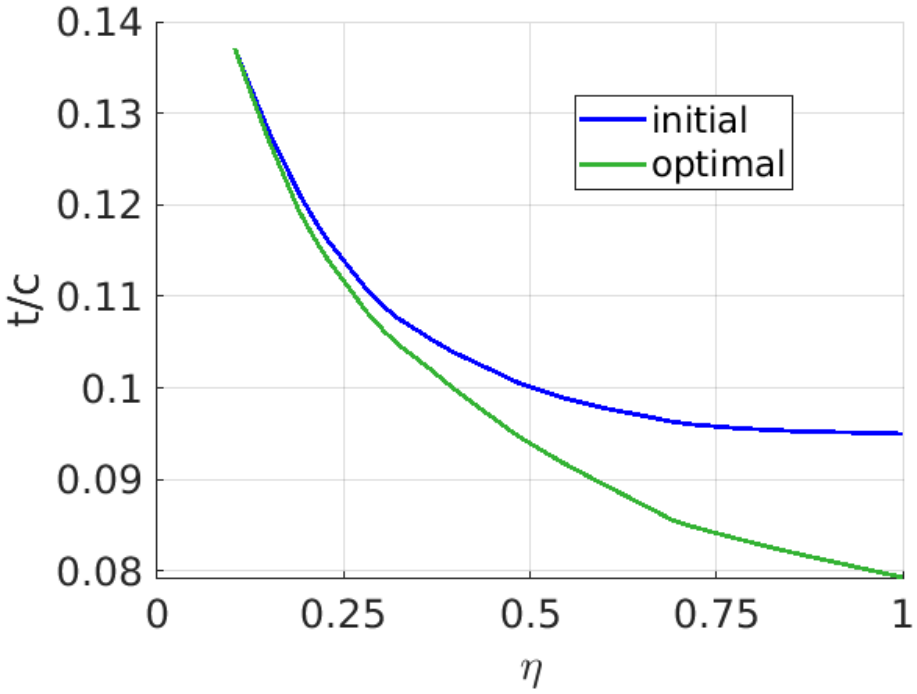

Figure 20 Wing t/c distribution for initial and optimal designs.

The reduction in the wing thickness is also evident in the airfoil plots shown in figure 21. However, airfoil shape changes also had a significant performance impact. In figures 22 and 23, it is evident that the shock wave of the CRM wing at its standard design condition is no longer observed on the improved design.

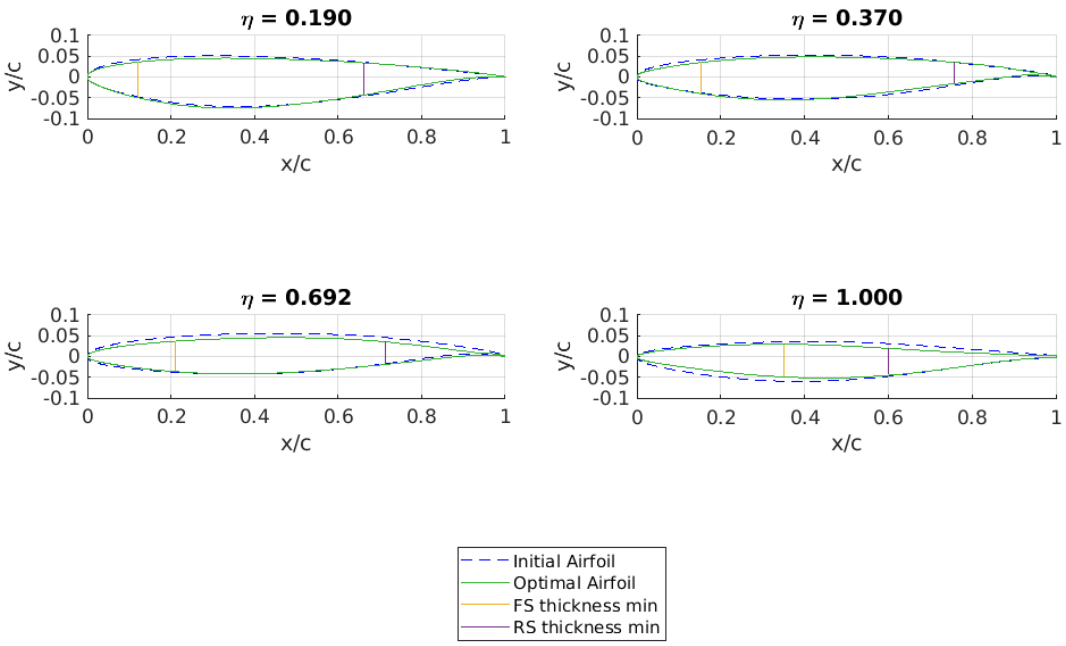

Figure 21 Airfoil comparison between initial and optimal designs.

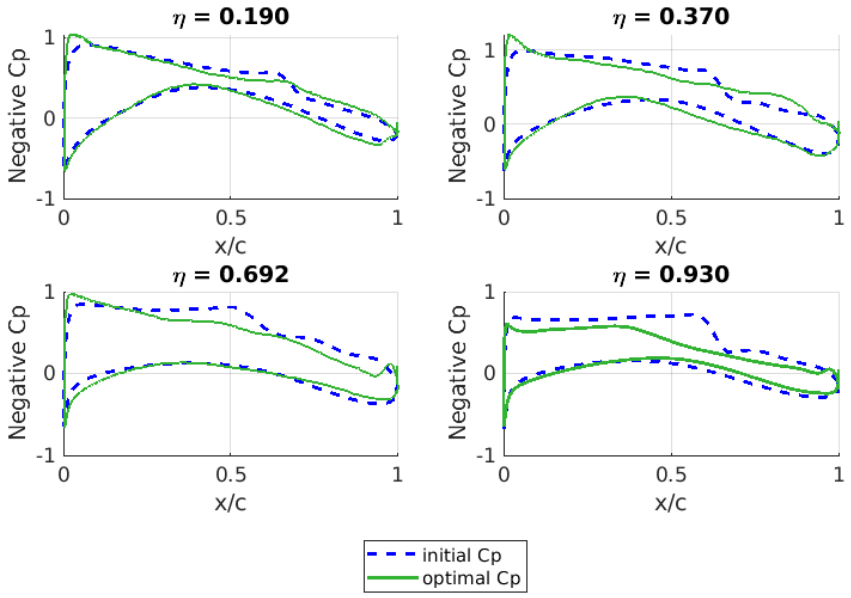

Figure 22 Wing pressure distribution comparison between initial and optimal designs.

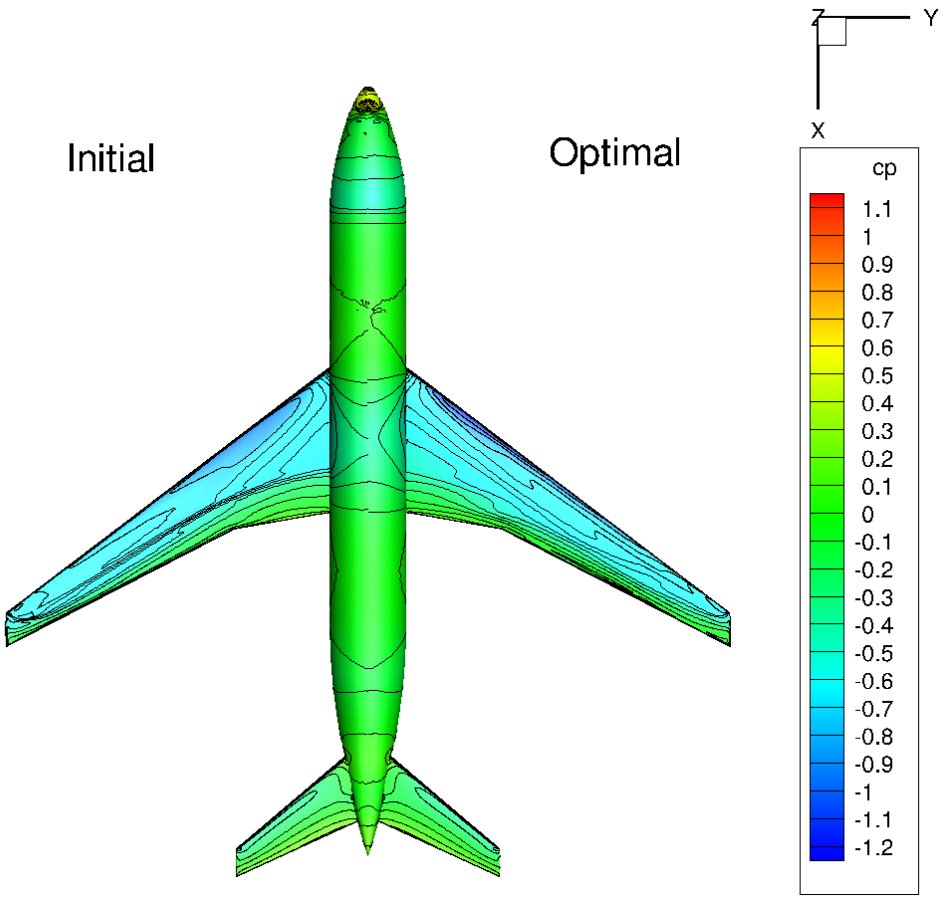

Figure 23 Pressure coefficient surface contour comparison between initial and optimal designs.

As described, these results are indicative of a successful aerostructural optimization, and demonstrate the viability and efficiency of the new MDO methodology on a large-scale optimization problem.

V. Conclusion

A new methodology has been developed for the aerostructural optimization of an aircraft wing at the preliminary design stage. This methodology employs a one-shot, global surrogate model of the structural sizing process, which is coupled to a high-fidelity flow solver and integrated into a coupled-adjoint formulation to enable gradient-based optimization. The intent of the method is to facilitate interdisciplinary collaboration, while at the same time taking full advantage of the coupled-adjoint method for efficient gradient-based optimization. Since the surrogate is trained only once, prior to the aerostructural optimization, the method is well suited for an industrial environment consisting of distinct disciplinary teams of experts, as the use of surrogate modeling is a very effective way of sharing tools while preserving disciplinary autonomy.

This new method has been implemented in an automated workflow using the Isight process integration software, in

which the NSU3D code is used for the aerodynamic analysis, and the S4Wing and OptiStruct codes are used for the structural sizing and optimization, and building of the structural surrogate. It has been shown that the construction of an adequate one-shot, global surrogate model of the structural sizing is achievable using a training data-set of 2500 sample points and an elliptical basis function (EBF) surrogate modeling technique. This result also bodes well for utilizing the method with higher-fidelity structural ROMs with a larger number of outputs. The potential of the overall MDO method has been demonstrated with results on the aerostructural optimization of the CRM wing with 122 design variables and 8 geometric constraints.

VI. Acknowledgments

This work was funded in part by a grant from Bombardier Aviation, Montreal, Canada. The authors are also very grateful for the assistance and input provided by Denis Walch, Aerospace Structures Engineer at Bombardier Aviation. Collaboration with the University of Wyoming was funded by a grant from the Dassault Systèmes US Foundation, and computational resources were provided by the Advanced Research Computing Center at the University of Wyoming https://doi.org/10.15786/M2FY47.

References

[1] Sobieszczanski-Sobieski, J., and Haftka, R., 'Multidisciplinary aerospace design optimization - Survey of recent developments,' *34th Aerospace Sciences Meeting and Exhibit*, 1996. doi:10.2514/6.1996-711, URL https://arc.aiaa.org/doi/abs/10.2514/6.1996-711.

[2] Mavriplis, D. J., 'Discrete adjoint-based approach for optimization problems on three-dimensional unstructured meshes,' *AIAA journal*, Vol. 45, No. 4, 2007, pp. 741–750. doi:10.2514/1.22743, URL https://doi.org/10.2514/1.22743.

[3] Martins, J., and Hwang, J. T., 'Multidisciplinary Design Optimization of Aircraft Configurations—Part 1: A modular coupled-adjoint approach.' , May 2016. URL http://mdolab.engin.umich.edu, lecture series. Von Karman Institute for Fluid Dynamics, Sint-Genesius-Rode, Belgium.

[4] Goertz, S., Ilic, C., Jepsen, J., Leitner, M., Schulze, M., Schuster, A., Scherer, J., Becker, R., Zur, S., and Petsch, M., 'Multi-Level MDO of a Long-Range Transport Aircraft Using a Distributed Analysis Framework,' *18th AIAA/ISSMO Multidisciplinary Analysis and Optimization Conference*, American Institute of Aeronautics and Astronautics, Denver, Colorado, 2017. doi:10.2514/6.2017-4326, URL https://arc.aiaa.org/doi/10.2514/6.2017-4326.

[5] Piperni, P., DeBlois, A., and Henderson, R., 'Development of a Multilevel Multidisciplinary-Optimization Capability for an Industrial Environment,' *AIAA Journal*, Vol. 51, No. 10, 2013, pp. 2335–2352. doi:10.2514/1.J052180, URL https://arc.aiaa.org/doi/10.2514/1.J052180.

[6] Martins, J. R. R. A., and Lambe, A. B., 'Multidisciplinary Design Optimization: A Survey of Architectures,' *AIAA Journal*, Vol. 51, No. 9, 2013, pp. 2049–2075. doi:10.2514/1.J051895, URL http://arc.aiaa.org/doi/10.2514/1.J051895.

[7] Tedford, N. P., and Martins, J. R. R. A., 'Benchmarking Multidisciplinary Design Optimization Algorithms,' *Optimization and Engineering*, Vol. 11, No. 1, 2010, pp. 159–183. doi:10.1007/s11081-009-9082-6, URL http://link.springer.com/10.1007/s11081-009-9082-6.

[8] Gray, J., Moore, K. T., Hearn, T. A., and Naylor, B. A., 'Standard Platform for Benchmarking Multidisciplinary Design Analysis and Optimization Architectures,' *AIAA Journal*, Vol. 51, No. 10, 2013, pp. 2380–2394. doi:10.2514/1.J052160, URL http://arc.aiaa.org/doi/10.2514/1.J052160.

[9] Chittick, I. R., and Martins, J. R. R. A., 'An Asymmetric Suboptimization Approach to Aerostructural Optimization,' *Optimization and Engineering*, Vol. 10, No. 1, 2009, pp. 133–152. doi:10.1007/s11081-008-9046-2, URL http://link.springer.com/10.1007/s11081-008-9046-2.

[10] Chittick, I. R., and Martins, J. R. R. A., 'Aero-structural optimization using adjoint coupled post-optimality sensitivities,' *Structural and Multidisciplinary Optimization*, Vol. 36, No. 1, 2008, pp. 59–70. doi:10.1007/s00158-007-0200-9, URL http://link.springer.com/10.1007/s00158-007-0200-9.

[11] Gazaix, A., Gallard, F., Ambert, V., Guénot, D., Hamadi, M., Grihon, S., Sarouille, P., Druot, T. Y., Brézillon, J., Gachelin, V., Plakoo, J., Desfachelles, N., Bartoli, N., Lefebvre, T., Gürol, S., Pauwels, B., Vanaret, C., and Lafage, R., 'Industrial Application of an Advanced Bi-level MDO Formulation to Aircraft Engine Pylon Optimization,' *AIAA Aviation 2019 Forum*, American Institute of Aeronautics and Astronautics, Dallas, Texas, 2019. doi:10.2514/6.2019-3109, URL https://arc.aiaa.org/doi/10.2514/6.2019-3109.

[12] Ganguli, R., and Rajagopal, S., 'Multidisciplinary Design Optimization of an UAV Wing Using Kriging Based Multi-Objective Genetic Algorithm,' *50th AIAA/ASME/ASCE/AHS/ASC Structures, Structural Dynamics, and Materials Conference*, American Institute of Aeronautics and Astronautics, Palm Springs, California, 2009. doi:10.2514/6.2009-2219, URL https://arc.aiaa.org/doi/10.2514/6.2009-2219.

[13] Shi, R., Liu, L., Long, T., Liu, J., and Yuan, B., 'Surrogate Assisted Multidisciplinary Design Optimization for an All-Electric GEO Satellite,' *Acta Astronautica*, Vol. 138, 2017, pp. 301–317. doi:10.1016/j.actaastro.2017.05.032, URL https://linkinghub.elsevier.com/retrieve/pii/S009457651631387X.

[14] Zhang, Y., Jia, D., Bontoft, E. K., and Toropov, V., 'Wing jig shape optimisation with gradient-assisted metamodel building in a trust-region optimisation framework,' *Structural and Multidisciplinary Optimization*, Vol. 65, No. 12, 2022, p. 350. doi:10.1007/s00158-022-03453-0, URL https://link.springer.com/10.1007/s00158-022-03453-0.

[15] Liu, H., Ong, Y.-S., and Cai, J., 'A survey of adaptive sampling for global metamodeling in support of simulation-based complex engineering design,' *Structural and Multidisciplinary Optimization*, Vol. 57, No. 1, 2018, pp. 393–416. doi:10.1007/s00158-017-1739-8, URL http://link.springer.com/10.1007/s00158-017-1739-8.

[16] Zhang, K.-S., Han, Z.-H., Li, W.-J., and Song, W.-P., 'Coupled Aerodynamic/Structural Optimization of a Subsonic Transport

Wing Using a Surrogate Model,' *Journal of Aircraft*, Vol. 45, No. 6, 2008, pp. 2167–2171. doi:10.2514/1.36047, URL https://arc.aiaa.org/doi/10.2514/1.36047.

[17] Long, T., Liu, L., Zhou, S., Wang, J., and Meng, L., 'Multi-Objective Multidisciplinary Optimization of Long-Endurance UAV Wing Using Surrogate Model in ModelCenter,' *12th AIAA/ISSMO Multidisciplinary Analysis and Optimization Conference*, American Institute of Aeronautics and Astronautics, Victoria, British Columbia, Canada, 2008. doi:10.2514/6.2008-5918, URL https://arc.aiaa.org/doi/10.2514/6.2008-5918.

[18] Kumano, T., Jeong, S., Obayashi, S., Ito, Y., Hatanaka, K., and Morino, H., 'Multidisciplinary Design Optimization of Wing Shape for a Small Jet Aircraft Using Kriging Model,' *44th AIAA Aerospace Sciences Meeting and Exhibit*, American Institute of Aeronautics and Astronautics, Reno, Nevada, 2006. doi:10.2514/6.2006-932, URL https://www.researchgate.net/publication/252259662_Multidisciplinary_Design_Optimization_of_Wing_Shape_for_a_Small_Jet_Aircraft_Using_Kriging_Model.

[19] Wunderlich, T., Dähne, S., Heinrich, L., and Reimer, L., 'Multidisciplinary Optimization of an NLF Forward Swept Wing in Combination with Aeroelastic Tailoring Using CFRP: DLR Contribution to the LuFo IV Joint Research Project AeroStruct,' *CEAS Aeronautical Journal*, Vol. 8, No. 4, 2017, pp. 673–690. doi:10.1007/s13272-017-0266-z, URL http://link.springer.com/10.1007/s13272-017-0266-z.

[20] Kaufman, M., Balabanov, V., Burgee, S. L., Giunta, A. A., Grossman, B., Haftka, R. T., Mason, W. H., and Watson, L. T., 'Variable-Complexity Response Surface Approximations for Wing Structural Weight in HSCT Design,' *Computational Mechanics*, Vol. 18, 1996, pp. 112–126. doi:https://doi.org/10.1007/BF00350530, URL https://link.springer.com/article/10.1007/BF00350530#citeas.

[21] Davies, C., Stelmack, M., Zink, P. S., De La Garza, A., and Flick, P., 'High Fidelity MDO Process Development and Application to Fighter Strike Conceptual Design,' *12th AIAA Aviation Technology, Integration, and Operations (ATIO) Conference and 14th AIAA/ISSMO Multidisciplinary Analysis and Optimization Conference*, American Institute of Aeronautics and Astronautics, Indianapolis, Indiana, 2012. doi:10.2514/6.2012-5490, URL https://arc.aiaa.org/doi/10.2514/6.2012-5490.

[22] Tianyuan, H., and Xiongqing, Y., 'Aerodynamic/Stealthy/Structural Multidisciplinary Design Optimization of Unmanned Combat Air Vehicle,' *Chinese Journal of Aeronautics*, Vol. 22, No. 4, 2009, pp. 380–386. doi:10.1016/S1000-9361(08)60114-4, URL https://linkinghub.elsevier.com/retrieve/pii/S1000936108601144.

[23] Sobieski, I. P., and Kroo, I. M., 'Collaborative Optimization Using Response Surface Estimation,' *AIAA Journal*, Vol. 38, No. 10, 2000, pp. 1931–1938. doi:10.2514/2.847, URL https://arc.aiaa.org/doi/10.2514/2.847.

[24] Chaussee, J., and Dervault, F., 'Knowledge Based Approach to Wing Weight and Stiffness Estimation at Early Stages of Aircraft Design,' *54th AIAA/ASME/ASCE/AHS/ASC Structures, Structural Dynamics, and Materials Conference*, American Institute of Aeronautics and Astronautics, Boston, Massachusetts, 2013. doi:10.2514/6.2013-1678, URL https://arc.aiaa.org/doi/10.2514/6.2013-1678.

[25] Wu, N., Mader, C. A., and Martins, J. R. R. A., 'A Gradient-based Sequential Multifidelity Approach to Multidisciplinary Design Optimization,' *Structural and Multidisciplinary Optimization*, Vol. 65, No. 4, 2022, p. 131. doi:10.1007/s00158-022-03204-1, URL https://link.springer.com/10.1007/s00158-022-03204-1.

[26] Kennedy, G. J., and Martins, J. R. R. A., 'A parallel aerostructural optimization framework for aircraft design studies,' *Structural and Multidisciplinary Optimization*, Vol. 50, No. 6, 2014, pp. 1079–1101. doi:10.1007/s00158-014-1108-9, URL http://link.springer.com/10.1007/s00158-014-1108-9.

[27] Mani, K., and Mavriplis, D. J., 'Adjoint-Based Sensitivity Formulation for Fully Coupled Unsteady Aeroelasticity Problems,' *AIAA Journal*, Vol. 47, No. 8, 2009, pp. 1902–1915. doi:10.2514/1.40582, URL https://arc.aiaa.org/doi/10.2514/1.40582.

[28] Elham, A., and van Tooren, M. J. L., 'Coupled adjoint aerostructural wing optimization using quasi-three-dimensional aerodynamic analysis,' *Structural and Multidisciplinary Optimization*, Vol. 54, No. 4, 2016, pp. 889–906. doi:10.1007/s00158-016-1447-9, URL http://link.springer.com/10.1007/s00158-016-1447-9.

[29] Wang, L., Shan, S., and Wang, G. G., 'Mode-pursuing sampling method for global optimization on expensive black-box functions,' *Engineering Optimization*, Vol. 36, No. 4, 2004, pp. 419–438. doi:10.1080/03052150410001686486, URL http://www.tandfonline.com/doi/abs/10.1080/03052150410001686486.

[30] Müller, J., and Shoemaker, C. A., 'Influence of Ensemble Surrogate Models and Sampling Strategy on the Solution Quality of Algorithms for Computationally Expensive Black-Box Global Optimization Problems,' *Journal of Global Optimization*, Vol. 60, No. 2, 2014, pp. 123–144. doi:10.1007/s10898-014-0184-0, URL http://link.springer.com/10.1007/s10898-014-0184-0.

[31] Yamazaki, W., and Mavriplis, D. J., 'Derivative-Enhanced Variable Fidelity Surrogate Modeling for Aerodynamic Functions,' *AIAA Journal*, Vol. 51, No. 1, 2013, pp. 126–137. doi:10.2514/1.J051633, URL https://doi.org/10.2514/1.J051633.

[32] Bartoli, N., Lefebvre, T., Dubreuil, S., Olivanti, R., Bons, N., Martins, J. R. R. A., Bouhlel, M.-A., and Morlier, J., 'An adaptive optimization strategy based on mixture of experts for wing aerodynamic design optimization,' *18th AIAA/ISSMO Multidisciplinary Analysis and Optimization Conference*, American Institute of Aeronautics and Astronautics, Denver, Colorado, 2017. doi:10.2514/6.2017-4433, URL https://arc.aiaa.org/doi/10.2514/6.2017-4433.

[33] Dufour, R., de Muelenaere, J., and Elham, A., 'Trajectory Driven Multidisciplinary Design Optimization of a Sub-Orbital Spaceplane Using Non-Stationary Gaussian Process,' *Structural and Multidisciplinary Optimization*, Vol. 52, No. 4, 2015, pp. 755–771. doi:10.1007/s00158-015-1267-3, URL http://link.springer.com/10.1007/s00158-015-1267-3.

[34] Bedonian, G., Hicken, J. E., and Forster, E., 'A gradient-enhanced partition-of-unity surrogate model and adaptive sampling strategy for non-analytic functions,' *Structural and Multidisciplinary Optimization*, Vol. 66, No. 7, 2023, p. 167. doi:10.1007/s00158-023-03620-x, URL https://link.springer.com/10.1007/s00158-023-03620-x.

[35] Fontana, J. E., Piperni, P., Yang, Z., and Mavriplis, D. J., 'Coupled Aerostructural Optimization using High-Fidelity Aerodynamics and Surrogate Modeling for the Structure,' *AIAA AVIATION 2022 Forum*, American Institute of Aeronautics and Astronautics, Chicago, IL & Virtual, 2022. doi:10.2514/6.2022-3359, URL https://arc.aiaa.org/doi/10.2514/6.2022-3359.

[36] Lambe, A. B., and Martins, J. R. R. A., 'Extensions to the Design Structure Matrix for the Description of Multidisciplinary Design, Analysis, and Optimization Processes,' *Structural and Multidisciplinary Optimization*, Vol. 46, No. 2, 2012, pp. 273–284. doi:10.1007/s00158-012-0763-y, URL http://link.springer.com/10.1007/s00158-012-0763-y.

[37] Mavriplis, D. J., and Mani, K., 'Unstructured mesh solution techniques using the NSU3D solver,' *AIAA Paper 2014-0081, 52nd Aerospace Sciences Meeting*, 2014. doi:10.2514/6.2014-0081, URL https://arc.aiaa.org/doi/abs/10.2514/6.2014-0081.

[38] Mavriplis, D. J., Fabiano, E., and Anderson, E., 'Recent Advances in High-Fidelity Multidisciplinary Adjoint-Based Optimization with the NSU3D Flow Solver Framework,' *55th AIAA Aerospace Sciences Meeting*, American Institute of Aeronautics and Astronautics, Grapevine, Texas, 2017. doi:10.2514/6.2017-1669, URL https://arc.aiaa.org/doi/10.2514/6.2017-1669.

[39] Marcelet, M., Peter, J., and Carrier, G., 'Sensitivity Analysis of a Strongly Coupled Aero-Structural System Using Direct and Adjoint Methods,' *12th AIAA/ISSMO Multidisciplinary Analysis and Optimization Conference*, American Institute of Aeronautics and Astronautics, Victoria, British Columbia, Canada, 2008. doi:10.2514/6.2008-5863, URL https://arc.aiaa.org/doi/10.2514/6.2008-5863.

[40] Fabiano, E., and Mavriplis, D., 'Adjoint-based aeroacoustic design-optimization of flexible rotors in forward flight,' *Journal of the American Helicopter Society*, Vol. 62, No. 4, 2017, pp. 1–17. doi:https://doi.org/10.4050/JAHS.62.042005, URL https://www.ingentaconnect.com/content/ahs/jahs/2017/00000062/00000004/art00005;jsessionid=3ijga6sficsao.x-ic-live-01#expand/collapse.

[41] Martins, J. R., 'A Coupled-Adjoint Method for High-Fidelity Aero-Structural Optimization,' PhD. dissertation, Stanford University, Dept. Aeronautics and Astronautics, Oct. 2002.

[42] Glauert, H., *The Elements of Aerofoil and Airscrew Theory*, Cambridge Universiy Press, London, UK, 1937.

[43] Gockel, M., and Corporation, M.-S., *MSC/NASTRAN Handbook for Superelement Analysis: MSC/NASTRAN Version 61*, MacNeal-Schwendler Corporation, 1981. URL https://books.google.com/books?id=ye5DAQAAIAAJ.

[44] Brooks, T. R., Kenway, G. K. W., and Martins, J. R. R. A., 'Benchmark Aerostructural Models for the Study of Transonic Aircraft Wings,' *AIAA Journal*, Vol. 56, No. 7, 2018, pp. 2840–2855. doi:10.2514/1.J056603, URL https://arc.aiaa.org/doi/10.2514/1.J056603.

[45] Mavriplis, D., 'Time Dependent Adjoint Methods for Single and Multi-disciplinary Problems,' , Sep. 2015. URL https://server.scientific-sims.com/cfdlab/scientific-sims/papers.html, 38th Advanced Computational

Fluid Dynamics. Adjoint methods and their application in Computational Fluid Dynamics, VKI Lecture Series, Von Karman Institute for Fluids Dynamics, Rhode St Genese, Belgium.

[46] Mavriplis, D. J., Fabiano, E., and Anderson, E., 'Recent advances in high-fidelity multidisciplinary adjoint-based optimization with the NSU3D flow solver framework,' *AIAA Paper 2017-1669, 55th AIAA Aerospace Sciences Meeting*, 2017. doi: 10.2514/6.2017-1669, URL https://arc.aiaa.org/doi/abs/10.2514/6.2017-1669.

[47] Walch, D., Tetreault, S., and Dervault, F., 'Smeared Stiffeners in Panel for Mesh Simplification at Conceptual Design Phase,' *54th AIAA/ASME/ASCE/AHS/ASC Structures, Structural Dynamics, and Materials Conference*, AIAA, Boston, Massachusetts, 2013. doi:https://doi.org/10.2514/6.2013-1809.

[48] Elsayed, M. S. A., Sedaghati, R., and Abdo, M., 'Accurate Stick Model Development for Static Analysis of Complex Aircraft Wing-Box Structures,' *AIAA Journal*, Vol. 47, No. 9, 2009, pp. 2063–2075. doi:10.2514/1.38447, URL https://arc.aiaa.org/doi/10.2514/1.38447.

[49] Bouhlel, M. A., Hwang, J. T., Bartoli, N., Lafage, R., Morlier, J., and Martins, J. R., 'A Python Surrogate Modeling Framework with Derivatives,' *Advances in Engineering Software*, Vol. 135, 2019. doi:10.1016/j.advengsoft.2019.03.005, URL https://linkinghub.elsevier.com/retrieve/pii/S0965997818309360.

[50] Mak, M., and Li, C., 'Elliptical basis function networks and radial basis function networks for speaker verification: a comparative study,' *IJCNN'99. International Joint Conference on Neural Networks. Proceedings (Cat. No.99CH36339)*, Vol. 5, 1999, pp. 3034–3039 vol.5. doi:10.1109/IJCNN.1999.836039.

[51] Mishra, A., Mani, K., Mavriplis, D., and Sitaraman, J., 'Time dependent adjoint-based optimization for coupled fluid–structure problems,' *Journal of Computational Physics*, Vol. 292, 2015, pp. 253–271. doi:https://doi.org/10.1016/j.jcp.2015.03.010, URL https://www.sciencedirect.com/science/article/pii/S0021999115001461.

[52] Brooks, T. R., Kenway, G. K., and Martins, J. R. R. A., 'Undeflected Common Research Model (uCRM): An Aerostructural Model for the Study of High Aspect Ratio Transport Aircraft Wings,' *35th AIAA Applied Aerodynamics Conference*, American Institute of Aeronautics and Astronautics, Denver, Colorado, 2017. doi:10.2514/6.2017-4456, URL https://arc.aiaa.org/doi/10.2514/6.2017-4456.

[53] Kenway, G., Kennedy, G., and Martins, J. R. R. A., 'Aerostructural optimization of the Common Research Model configuration,' *15th AIAA/ISSMO Multidisciplinary Analysis and Optimization Conference*, American Institute of Aeronautics and Astronautics, Atlanta, GA, 2014. doi:10.2514/6.2014-3274, URL https://arc.aiaa.org/doi/10.2514/6.2014-3274.

[54] Klimmek, T., 'Parametric Set-Up of a Structural Model for FERMAT Configuration for Aeroelastic and Loads Analysis,' *Journal of Aeroelasticity and Structural Dynamics*, , No. 2, 2014, pp. 31–49. doi:10.3293/asdj.2014.27, URL https://doi.org/10.3293/asdj.2014.27.

[55] Gill, P. E., Murray, W., and Saunders, M. A., 'SNOPT: An SQP Algorithm for Large-Scale Constrained Optimization,' *SIAM Journal on Optimization*, Vol. 12, No. 4, 2002, pp. 979–1006. doi:10.2307/20453604.

[56] Brooks, T., 'Design Optimization of Flexible Aircraft Wings Using Tow-steered Composites,' PhD, University of Michigan, 2018.

[57] Vassberg, J. C., Tinoco, E. N., Mani, M., Rider, B., Zickuhr, T., Levy, D. W., Brodersen, O. P., Eisfeld, B., Crippa, S., Wahls, R. A., Morrison, J. H., Mavriplis, D. J., and Murayama, M., 'Summary of the Fourth AIAA Computational Fluid Dynamics Drag Prediction Workshop,' *Journal of Aircraft*, Vol. 51, No. 4, 2014, pp. 1070–1089. doi:10.2514/1.C032418, URL https://arc.aiaa.org/doi/10.2514/1.C032418.

[58] Tashnizi, E. S., Taheri, A. A., and Hekmat, M. H., 'Investigation of the adjoint method in aerodynamic optimization using various shape parameterization techniques,' *Journal of the Brazilian Society of Mechanical Sciences and Engineering*, Vol. 32, No. 2, 2010. URL https://www.scielo.br/j/jbsmse/a/L9SNF6W6N9MLDkByN4L4jMc/.